A Late Pleistocene coastal ecosystem in French Guiana was hyperdiverse relative to today

Pierre-Olivier Antoine, Linde N Wieringa, Sylvain Adnet, Orangel Aguilera, Stéphanie C Bodin, Stephen Cairns, Carlos A Conejeros-Vargas, Jean-Jacques Cornée, Žilvinas Ežerinskis, Jan Fietzke, et al.

Proceedings of the National Academy of Sciences USA
(Doi: http://dx.doi.org/10.1073/pnas.2311597121)

A Late Pleistocene coastal ecosystem in French Guiana was hyperdiverse relative to today

Pierre-Olivier Antoine[a,*], Linde N. Wieringa[a], Sylvain Adnet[a], Orangel Aguilera[b], Stéphanie C. Bodin[c], Stephen Cairns[d], Carlos A. Conejeros-Vargas[e], Jean-Jacques Cornée[f], Žilvinas Ežerinskis[g], Jan Fietzke[h], Natacha O. Gribenski[i], Sandrine Grouard[j], Austin Hendy[k], Carina Hoorn[l], Renaud Joannes-Boyau[m,n], Martin R. Langer[o], Javier Luque[p], Laurent Marivaux[a], Pierre Moissette[q], Kees Nooren[l], Frédéric Quillévéré[r], Justina Šapolaitė[g], Matteo Sciumbata[l,s], Pierre G. Valla[t], Nina H. Witteveen[l], Alexandre Casanova[u], Simon Clavier[v], Philibert Bidgrain[u], Marjorie Gallay[w], Mathieu Rhoné[w] & Arnauld Heuret[f,u]

[a] Institut des Sciences de l'Évolution de Montpellier, Univ Montpellier, CNRS, IRD, 34095 Montpellier, France

[b] Fluminense Federal University, Paleoecology and Global Changes Laboratory, Niterói, Rio de Janeiro, Brazil

[c] Department of Paleoanthropology, Senckenberg Research Institute, Frankfurt am Main, Germany

[d] Department of Invertebrate Zoology, Smithsonian Institution, National Museum of Natural History, Washington DC, USA

[e] Departamento de Ciencias del Mar y Limnología, Universidad Nacional Autónoma de México, Coyoacán, Ciudad de México, México

[f] Géosciences Montpellier, Univ Montpellier, CNRS, 34095 Montpellier, France

[g] Mass Spectrometry Laboratory, Center for Physical Sciences and Technology, Vilnius, Lithuania

[h] GEOMAR, Helmholtz Centre for Ocean Research Kiel, Kiel, Germany

[l] Institute of Geological Sciences and Oeschger Centre for Climate Change Research, University of Bern, Bern, Switzerland

[j] Archéozoologie et Archéobotanique – Sociétés, Pratiques et Environnements, CNRS, Muséum National d'Histoire Naturelle, Paris, France

[k] Invertebrate Paleontology, Natural History Museum of Los Angeles County, Los Angeles, USA

[l] Institute for Biodiversity and Ecosystem Dynamics, Universiteit van Amsterdam, Amsterdam, The Netherlands

[m] Geoarchaeology and Archaeometry Research Group, Southern Cross University, Lismore, Australia

[n] Centre for Anthropological Research, University of Johannesburg, Johannesburg, South Africa

[o] Institute für Geowissenschaften, Paläontologie, Universität Bonn, Bonn, Germany

[p] Cambridge University Museum of Zoology, Department of Zoology, Cambridge, United Kingdom

[q] Department of Historical Geology-Paleontology, National and Kapodistrian University of Athens, Panepistimiopolis, Zografou, 15784 Athens, Greece

[r] Laboratoire de Géologie de Lyon-Terre, planètes, environnement, Université Claude Bernard Lyon 1, ENS de Lyon, CNRS, Villeurbanne, France

[s] Amsterdam Institute for Life and Environment (A-LIFE), section Systems Ecology, Vrije Universiteit, Amsterdam, The Netherlands

[t] Institut des Sciences de la Terre, Université Grenoble Alpes, Université Savoie Mont Blanc, CNRS, IRD, IFSTAR, Université Gustave Eiffel, Grenoble, France

[u] Département Formation et Recherche Sciences et Technologie, Université de Guyane, Cayenne, Guyane

[v] Onikha, Kourou, Guyane

[w] Office de l'Eau de Guyane, Cayenne, Guyane

*To whom correspondence may be addressed (pierre-olivier.antoine@umontpellier.fr)

Competing Interest Statement: The authors declare no competing financial interests.

Classification: Biological Science - Evolution.

Abstract. Warmer temperatures and higher sea-level than today characterized the Last Interglacial interval (Pleistocene, 128–116 thousand years ago [ka]). This period is a remarkable deep-time analog for temperature and sea-level conditions as projected for 2100 AD yet there has been no evidence of fossil assemblages in the equatorial Atlantic. Here we report foraminifer, metazoan (mollusks, bony fish, bryozoans, decapods, and sharks among others) and plant communities of coastal tropical marine and mangrove affinities, dating precisely from a *ca.* 130–115 ka time interval near the Equator, at Kourou, in French Guiana. These communities include *ca.* 230 recent species, some being endangered today and/or recorded for the first time as fossils. The hyperdiverse Kourou mollusk assemblage suggests stronger affinities between Guianese and Caribbean coastal waters by the Last Interglacial than today, questioning the structuring role of the Amazon Plume on tropical Western Atlantic communities at the time. Grassland-dominated pollen, phytoliths and charcoals from younger deposits in the same sections attest to a marine retreat and dryer conditions during the onset of the last glacial (*ca.* 110–50 ka), with a savanna-dominated landscape and episodes of fire. Charcoals from the last millennia suggest human presence in a mosaic of modern-like continental habitats. Our results provide key information about the ecology and biogeography of pristine Pleistocene tropical coastal ecosystems, especially relevant regarding the—widely anthropogenic—ongoing global warming.

Significance Statement. The Last Interglacial interval (128–116 ka) is a remarkable deep-time analog for temperature and sea-level conditions as projected for 2100 AD, that had not been documented in the equatorial Atlantic thus far. Here we report hyperdiverse fossil communities of coastal marine and mangrove affinities, dating back from this interval and unearthed at the Europe's Spaceport in Kourou, French Guiana. Mollusk assemblages suggest stronger ecological affinities between Guianas and the Caribbean than today. Grassland-dominated pollen, phytoliths, and charcoals from younger deposits in the same sections attest to a marine retreat and dryer conditions during the Last Glacial Period (100–50 ka). These records provide key ecological and biogeographic information about Late Pleistocene tropical coastal ecosystems prior to human influence.

Keywords: French Guiana; ancient ecosystems; past biodiversity; Last Interglacial; climate change

Introduction

During the last two million years, climatic oscillations induced environmental fluctuations that resulted in drastic changes in biotic distribution all over the globe (1–3). For example, global sea-level fluctuated up to 120 m between glacial and interglacial maxima, primarily forced by orbital cycles (4, 5). Such fluctuations led to iterative emergences and drownings of low-elevation coastal areas, with deep consequences on marine taxa (3, 6). The Last Interglacial interval (LIG; Marine Isotope Stage [MIS] 5e; 128–116 ka) is characterized by up to 4–6 m higher sea-level conditions and overall climatic conditions 2–4°C warmer than today (7–10), making this period a deep-time analog for temperature and sea-level conditions as projected for 2100 AD (11). Despite the existence of numerous data available worldwide, very little is known about LIG low-land biotic assemblages near the Equator, their ecology and biogeography, more especially in the Atlantic region (8, 10–14) (Fig. 1A; *SI Dataset 1*). This gap notably prevents from characterizing the tropical Atlantic biotic communities in the penultimate Earth's warm episode (11, 15–17).

The Guianas comprise a vast territory (*ca.* 2.5 million-km2) near the Equator in South America. Today, this region shelters high levels of taxonomic diversity in both terrestrial and aquatic ecosystems (18–20), but we know almost nothing about its past biodiversity (21, 22). Guianese coastal areas are covered by mangrove vegetation and tidally-influenced river banks whilst, more inland, herbaceous swamps and savannas are followed by marsh and evergreen woodlands (23). This dense vegetation further hampers access to potential fossil-yielding outcrops. Guianese coasts are strongly impacted by a huge flux of surface waters of Andean-Amazonian origin (24), termed the Amazon Plume (AP). This northwestward flux strongly structures the composition of recent tropical Western Atlantic biotic communities, without a clue about its role in the past (24–26).

Here we report a hyperdiverse marine LIG assemblage, separated by a hiatus from younger continental fossil communities, in a section spanning the last *ca.* 130 ka. This succession was uncovered during the titanic earthworks that were undertaken in 2015–2020 for the Ariane 6 ELA4 launching pad (here KOU-AR6) at Europe's Spaceport, Kourou, French Guiana (FG; Fig. 1B–D). Our research team includes many specialists from the fields of paleontology and paleobotany to fully reconstruct these ecosystems by using as many different taxonomic groups as possible. As a result, these fossil communities comprise over 270 taxa of foraminifers, metazoans (mollusks, bryozoans, decapods, ray-finned fish, and selachians among others), and plants, further providing a first glimpse into the composition of equatorial coastal ecosystems (marine and terrestrial), during both the LIG and the Last Glacial Period (LGP, *ca.* 115–12 ka).

These ancient ecosystems predate human arrival in the Guianas [*ca.* 10 ka BP (27–29)]. They can contribute to testing: i) the regional effects of the global marine retreat related to the LGP; ii) the behavior of equatorial Atlantic biodiversity during the LIG; iii) the deep history of the AP as a major structuring element of Western Atlantic marine communities; and iv) the relative abundance of now critically-endangered marine taxa, in the absence of human footprint.

Results and interpretation

Pleistocene–Holocene sections at the Ariane 6 launch pad, Kourou, FG. Six trenches and ditches were excavated and investigated for their paleontological content over a 0.5 km2 surface in 2019 (KOU-AR6-01 to -05) and 2021 (KOU-AR6-06; Fig. 1C). Common and salient features in these geological sections enabled us to build an 8-m thick composite section (*SI Appendix*, Figs. S1–S6, S11). The base of the section is formed by the top of a Paleoproterozoic granitoid (crystalline basement), which coincides with current sea-level (-1/+1 m). The granitoid is overlain by around 0.5 m of pink saprolites (chemically-weathered granitoids), followed by a 7-m thick sedimentary deposit (Fig. 1D; *SI Appendix*, Fig. S11). The latter deposit includes three successive units with an erosional base (Units A–C). Based on its fossil content (see below), the lowermost part of this sedimentary ensemble (Unit A, around 4-m thick) is unambiguously of marine origin and referable to the Middle–Late Pleistocene Coswine Formation (Fm.), documented in coastal areas of FG (30, 31).

In all trenches, the fossil-rich ensemble starts by marine deposits (Unit A lying on previously-emerged bedrock, transformed into paleosols higher up and topped by an emersion surface, thereby documenting a transgressive/regressive sedimentary cycle). More specifically, Unit A consists of a basal grey oyster-rich conglomerate, transgressive and overlain by grey silty clays (1.5 m). It is covered by a khaki conglomerate in trenches KOU-AR6-03 and -05, with quartz pebbles and oxidized elements, laterally equivalent to khaki or ocher sands in other trenches. Both conglomerates yield calcareous, phosphatic and siliceous, or carbonized marine macrofossils, plus foraminifers and palynomorphs (*SI Appendix*). Above the khaki conglomerate/sand, a regressive sequence starts with 1.5 m of variegated silty paleosols (blueish and ocher or beige and yellow), yielding only siliceous and phosphatized marine fossils (brachiopods and fish; KOU-AR6-06) attesting to their marine origin, with a subsequent weathering due to pedogenesis. These variegated silts become reddish upward and turn into either an iron crust (at KOU-AR6-03, -04 and 05) or a yellow quartz-rich siltite, yielding only continental palynomorphs and phytoliths (at KOU-AR6-06) and topping Unit A. Above it, Unit B is characterized, in all trenches, by around 1.5 m of brownish-orange, grey or yellow silts of continental origin. At KOU-AR6-06, Unit B begins with a 15-cm thick dark microconglomeratic peat (around

2.5 m above sea-level [PN-15a-b pollen and phytolith samples]; Fig. 1D). The top of this continental sequence is cut or weathered and replaced by modern soils and human-disturbed surfaces in most of the studied sections. Nevertheless, the KOU-AR6-04 section, culminating 2–4 m above all other investigated sections (*SI Appendix*, Fig. S11), provides information on a third unit of fluvial origin, here termed Unit C. This unit consists of 2.5-m thick beige-brownish coarse sands intercalated with charcoal-rich microconglomeratic lenses and channels.

Age constraints on the KOU-AR6 sections. Nineteen samples were dated through independent proxies to estimate the ages of Unit A and C (*SI Appendix*, Tables S2–S6). From the base of Unit A (basal conglomerate), aragonitic Astrangia corals were dated by U-Th at 131±15 ka by laser ablation and by U-Th at a maximum age of 135.8±1.1 ka by conventional solution MS-ICP-MS (Fig. 1D). Higher up in Unit A, quartz-rich silts located 1.7 m above the base of the Coswine Fm. at KOU-AR6-06 were dated through optically-stimulated luminescence (OSL) with a minimum age estimate of 104.6±17.9 ka (sample OSL-2). Coswine clays formed a transgressive sequence around the Middle–Late Pleistocene transition (30, 31), further documenting the highest sea-level during the LIG [MIS 5e: 128–116 ka (9)], and reaching 4–6 m above the modern sea-level (8, 10). At the top of Unit A, OSL-1, a sample of ocher to beige clayey silts situated 1.1 m above OSL-2, was constrained with a minimum age estimate of 119.7±10.2 ka through OSL dating (corresponding possibly to MIS 5e or to the glacial stadial MIS 5d). For Unit B, there is no radioisotopic dating available, and its age must be bracketed. Two in-situ charcoal samples from successive continental fluvial channels at KOU-AR6-04 provided consistent 14C ages at 47053±572 and 43091±284 calibrated years Before Present [cal BP], dating the base and the lower part of Unit C, respectively (*SI Appendix*, Table S6). This time span falls within MIS 3, just preceding the LGM within the LGP (9, 32). Drastic climatic changes are recorded during this interval at high and mid-latitudes, but climatic models do consider that no seasonal temperature shift occurred between MIS 3 and the LGM at the Equator (33). The Holocene marine Demerara clays are not recorded in the investigated loci (30, 31). Finally, the two successive riverine channels situated just below the surface at KOU-AR6-04 (top of Unit C) were dated based on charcoals and yielded 14C ages of 1938±120 and 804±55 cal BP (Fig. 1D). At that time, human settlement and land use are well-documented locally (34, 35). Accordingly, the time intervals documented in the KOU-AR6 sections would be *ca.* 130–115 ka (Unit A, marine), *ca.* 110–*ca.* 50 ka (Unit B, continental) and 47–1 ka (Unit C, continental).

The biotic communities at KOU-AR6 (Pleistocene to Holocene)

All the fossil specimens from the sampled sections are referable to living species, i.e., no extinct taxon is documented thus far at KOU-AR6.

Unit A (ca. 130–115 ka), mangrove to shallow marine environment. Unit A (Fig. 4A) documents a very short high sea-level interval spanning the LIG. Based on our chronological constraints, this is most likely MIS 5e, 128–116 ka (9). This sequence yielded hyperdiverse assemblages comprising 229 distinct taxa belonging to a wide array of phyla, including foraminifers, mollusks, ray-finned fish, bryozoans, decapods, and sharks among others (Fig. 2), but also plants (charcoals, phytoliths, and pollen; Fig. 3) derived from nearby coastal habitats. In general, mollusks and decapods dominate over other groups, with perfectly-preserved delicate shells, pointing to low-energy habitats and preservation in-situ.

Foraminifer communities (*SI Appendix*, Table S7) are mainly composed of hyaline-perforate benthic taxa (Fig. 2A–C), indicative for shallow intertidal mangrove and subtidal environments (11 species), and one individual of planktonic foraminifer (Fig. 2D). The smallest benthic species (*Nonion subturgidum*, *Elphidium magellanicum*, *Cerebrina claricerviculata*, and *Fursenkoina* sp.) usually live in low-oxygenated sediments, while other ones tolerate low-salinity conditions and potentially occur in mangrove habitats and estuaries with variable salinity conditions (*Ammonia*). All other benthic foraminifers are comparatively shallow marine, subtidal taxa, usually occurring in nearshore shallow-water environments with algae or seagrass vegetation. The open ocean influence was probably low. The foraminifers found in all trenches strongly recall the associations observed in a mangrove estuary in northern Brazil, with a significant marine tidal influence (36).

Sponges are only represented by *Entobia* boreholes in oyster shells (Fig. 2E). Cnidarians are documented by the octocorallian gorgonian *Pacifigorgia*, at KOU-AR6-06 (Fig. 2G) and >1700 specimens of a single scleractinian species, *Astrangia rathbuni*, either growing as solitary corallites or small colonies (Fig. 2F). *Astrangia rathbuni* was recognized in all sampled marine levels, with a much higher density at KOU-AR6-06 than in other trenches (*SI Appendix*, Table S8).

The trenches KOU-AR6-01, -03 and -05 yielded 19 species of bryozoans, mostly typical of tropical shallow waters. Most of these taxa also occur in the present-day coastal waters of Brazil [e.g., (37, 38)]. Warm-water genera (*Biflustra*, *Steginoporella*, *Antropora* and *Nellia*) are well represented in both recent and fossil Kourou records. The predominance of encrusting forms suggests a shallow depositional environment affected by freshwater influxes associated with increased turbidity, as in mangrove and oyster-rich settings (39).

Around 200 calcareous tubes of unidentified polychaete worms are documented in the marine sequence of all trenches. Siliceous shells of a single brachiopod taxon (*Discradisca antillarum*) are recorded at Kourou, with hundreds of specimens over the entire marine unit and in all sampled trenches.

Mollusks vastly dominate other phyla in both taxonomic diversity and specimen numbers (Fig. 2L–Y). They include two species of scaphopods (rare), 35 species of bivalves and 50 species of gastropods. Bivalves and snails are recorded by thousands of individuals in all marine levels that were sampled, with shallow water *Costoanachis avara* (Fig. 2S), *Sheldonella bisulcata* (Fig. 2N), and *Chione cancellata* (Fig. 2W) most abundant. In terms of richness and evenness, KOU-AR6-03 is most diverse with 59 species (*SI Appendix*, Table S10). The state of preservation is exquisite for several species which retain colored patterns visible to the naked eye [e.g., *Vitta* (Fig. 2Q), *Pilsbryspira*] or revealed under UV light [e.g., *Crassinella*, *Olivella*; Fig. 2Y]. Most molluscan taxa have affinities to intertidal and shallow subtidal sands, muds, or rocks and several species are characteristic of mangrove habitats (e.g., *Vitta virginea*, *Isognomon radiatus*).

The crustacean arthropods are particularly dominant at Kourou, with thousands of specimens retrieved from the sediments, all belonging to either barnacles (balanomorph cirripeds), crabs or shrimps (decapods). The barnacles are notably represented by a large amount of disconnected wall plates of *Amphibalanus*, and a single complete specimen (Fig. 2Z). The decapods are represented mostly by hundreds of isolated claw fragments, mainly of mobile and fixed fingers (*SI Appendix*, Table S11). The decapods comprise eight morphotypes, including two species of mud shrimps (Fig. 2A'–D'), three species of false crabs, or anomurans (Fig. 2E'– F'), and three species of true crabs, or brachyurans (Fig. 2G'–J'). Anomurans include filter feeders found in reefs, under rocks, shell beds, or mangroves. Small claw fragments further document a possible paguroid. The overall decapod association indicates proximity to mangroves, with soft sediments hosting *Neocallichirus* mud shrimps (feeding on seagrass and algae) and purse crabs *Persephona*. This association points to intertidal–subtidal tropical to temperate waters (0–50 m), with Western Atlantic, Caribbean, and tropical Eastern Pacific affinities (*Persephona*).

Echinoderms were retrieved in high numbers in all marine samples, nevertheless pointing to a low taxonomic diversity (three species). The echinoderm community is overdominated by the Atlantic purple sea urchin *Arbacia punctulata* (Fig. 2K') in all sampled levels and trenches (*SI Appendix*, Table S12). In stark contrast, we retrieved only a few dozens of test fragments of two unidentified heart urchins and two plates of an astropectinid sea star.

No marine mammals or seabirds were preserved, but elasmobranch (sharks and rays; Fig. 2L'–O') were identified in all trenches: four species of rays (whipray, eagle ray, saw fish, and cownose ray) and seven species of sharks, including smalltail, daggernose, sharpnose, and lemon sharks, as well as small scoophead hammer sharks and a nurse shark. Daggernose sharks and whiprays dominate the elasmobranch fauna in terms of specimens and occurrences (*SI Appendix*, Table S13). Bony fish are dominantly documented by otoliths (Fig. 2P'–T'), but also by bones and teeth (Fig. 2U'–W'), belonging to 35 species (*SI Appendix*, Table S14). Sciaenid perciforms (16 species, with five distinct *Stellifer*) and ariid siluriforms (eight species) widely outnumber other

taxonomic groups in the sample. KOU-AR6-03 is by far the richest locality, with 32 species; *SI Appendix*, Table S14). Thirteen species are recognized in two or three localities, pointing to a certain heterogeneity between the samples.

Plant composition and diversity in the marine unit is revealed by fossil charcoals, pollen, spores, and phytoliths (Fig. 3; *SI Appendix*, Tables S15–17). As for charcoals, red mangrove (cf. *Rhizophora* sp.), boarwood (cf. *Symphonia globulifera*) and two representatives of Chrysobalanaceae and Myrtaceae were recognized. At KOU-AR6-06, the base of the same unit yielded phytoliths referable to unidentified woody eudicot and Asteraceae, in PN9A and PN9C pollen samples, respectively. The corresponding palynological assemblage (Fig. 3A–I), with a low pollen concentration (around 700 grains.cm^{-3}), is dominated by *Rhizophora* pollen (80 %), followed by spores of the mangrove fern *Acrostichum* (3.5 %). No *Avicennia* pollen grains were found. Pollen of tree species accounts for 9 % of the pollen sum, and reflects the influx of hinterland and lowland (swamp) forest trees (40). Herb and vine pollen is relatively rare (5 %) and dominated by Poaceae and Asteraceae. Asteraceae pollen grains were only found in the PN9C sample, also containing one Asteraceae phytolith. The top of this unit has been comprehensively sampled at KOU-AR6-06 for palynomorphs and phytoliths (samples PN10–14; *SI Appendix*, Table S16). PN10–13 only provided a few phytoliths and PN10–14 was also devoid of palynological content. Grass phytoliths first occur at PN12 (dated at 104.6±17.9 ka, OSL-2), with a panicoid cross and a bilobate [C3 and C4 grasses (41, 42)], plus a fused and two rugose spheroids (woody eudicots). PN14 yielded phytolith assemblages dominated by grass phytoliths (70 %), as in PN15A-B (base of Unit B, see below).

Unit B (ca. 110 –50 ka), coastal savanna and dry forest. Only plant remains were retrieved in this unit.

Tree charcoals were identified at KOU-AR6-04 Base (Fig. 3Y; *SI Appendix*, Table S15). The assemblage comprises notably *Hadroanthus* cf. *serratifolius* (ipê) and a close relative, cf. *Drypetes* sp., *Pterocarpus*-like Leguminosae, red mangrove, as well as unidentified Melastomataceae, Myrtaceae-like dicots. Today, these taxa represent trees and shrubs from the primary, riverine or dry forest, savanna or mangrove and suggest distinct vegetation succession stages at *ca.* 47 ka *cal* BP.

The phytolith assemblages counted in the basal dark peat at KOU-AR6-06 (Fig. 3R –X) are dominated by grasses (65 %) in both PN15A and PN15B with 65 % grass, 31 and 17 % woody eudicots, respectively, and almost no palm phytoliths (<1 %). Most grass phytoliths encountered are from Panicoideae and Bambusoideae (*SI Appendix*, Table S16; Fig. S12). Bilobates and rondels are also common, produced by a wide array of monocot grasses (41, 42). Phytoliths from Pooideae (wavy trapezoids) and Chloridoideae (squat saddles) are rare (<1 %). Strikingly, a high percentage of phytoliths were burnt (28 %),

especially specimens of Cyperaceae, *Heliconia* and Zingiberales. This assemblage suggests that a savanna vegetation had started growing locally way before 50 ka and spread around and settled sustainably. Previous phytolith studies showed that the natural vegetation of seasonally-flooded/coastal Holocene savannas in FG consisted of Cyperaceae, Marantaceae and *Heliconia* herbs and panicoid and oryzoid grasses, with an overall high abundance of grass phytoliths (43).

The pollen concentration of the PN15 sample is much higher than in Unit A (around 20,600 grains.cm^{-3}), with a high relative abundance of Poaceae (49 %) and Spermacoceae (36 %) pollen, indicative of open and disturbed vegetation (Fig. 3L–Q) prior to 45 ka *cal* BP in the ELA4 area (Fig. 4B). Many Poaceae pollen grains are relatively large (50–64 µm), furthering the presence of Panicoideae and Bambusoideae grass phytoliths. Mangrove (2.4 %) and tree (3.5 %) pollen grains are rare (*SI Appendix*, Table S17). Conversely, the large amount of charred plant fragments ("microcharcoals") in the pollen slides is notable. The high number of macro-charcoals and high percentage of burned phytoliths indicate recurring fires at the site during the concerned time interval, i.e., prior to 47 ka *cal* BP (age of the base of the overlying Unit C; see below), and further consistent with a glacial stadial (MIS 4: 72–58 ka; Fig. 4D).

Unit C *(47–1 ka)*, dry/swamp forest and savanna to coastal savanna and chenier plain. Only macroscopic charcoals were hand-picked at KOU-AR6-04, in several levels from Unit C, spanning the 47–1 ka time interval (MIS 3c–1). More than 60 fragments, some of them from tree stumps, were retrieved in a brown conglomerate ("Mid"), ^{14}C-dated at 47053±572 *cal* BP. They attest to the most speciose tree community uncovered here through charcoals, with at least 15 distinct tree taxa (*SI Appendix*, Table S15). *Mouriri* sp. is the most abundant tree, followed by *Chaunochiton kappleri* and a close relative, two close allies of *Stryphnodendron*, two unidentified Chrysobalanaceae, Lecythidaceae, cf. Anacardiaceae/Burseraceae and ipê. Just above, floodplain deposits and a silty litter dated at 43091±284 *cal* BP yielded charcoals of unidentified affinities and bootlace tree, respectively. The top levels, dated from the last millennia (^{14}C ages of 1938±120 and 804±55 *cal* BP), yielded charcoals of unidentified Anacardiaceae/Burseraceae, hog plum, cf. Chrysobalanaceae, *Mabea* sp. in the older layer and bootlace tree, Rubiaceae anatomically close to batahua, as well as unidentified Chrysobalanaceae and Leguminosae in the younger one. Pollen and phytoliths were neither sampled nor investigated in Unit C, except for the last millennia (34).

Local landscape evolution since the LIG (Fig. 4A–C)

The marine unit represented in Unit A (Fig. 4A) documents a very short high sea-level interval spanning the LIG [most likely MIS 5e, 128–116 ka (9)]. *Rhizophora* trees and *Acrostichum* ferns nowadays only thrive in stable and mature mangroves (44). Their

dominance in the pollen assemblages (including pollen clumps) and as charcoals at the base of Unit A suggests that a mangrove ecosystem occurred in the close surroundings (*SI Appendix, Tables S15-16*). Pollen recovery further attests to the existence of montane (e.g., *Alnus*, probably Andean-sourced) and lowland swamp-forest trees, herb, and vines. This is supported by the recognition of dry-forest and back-mangrove tree charcoals (Chrysobalanaceae and Myrtaceae; Fig. 4A). Aquatic communities confirm the proximity of a mangrove belt (e.g., mangrove oysters, decapods, and foraminifers), with shallow-water marine habitats occurring near the sampling points (around 5-m depth), as supported by the co-occurrence of many mollusks. A certain habitat disparity can be inferred from coeval samples, with softer substrates at KOU-AR6-01 than at other loci (abundant spatangoid urchins) or more wave- or tide-related energy in KOU-AR6-06 and -05 Top than anywhere else—high proportion of broken specimens and solitary corallites—, thereby pointing to disturbed settings. This landscape strongly recalls the environments of Marajó Island in the Amazon delta and marginal islands with strong marine and tidal influence, as furthered by the co-occurrence of various bony fish taxa with ana-, amphi- or catadromous life cycles (*SI Appendix*, Table S14). Contrastingly, this type of highly-speciose shallow-water environments is not recorded in FG today (19, 45). The local and regional topographies at our sites are consistent with the ocean being open at the northeast, with terra-firma forests to the southwest (Fig. 1, Fig. 4A). Detrital elements sourced from the continent, through small freshwater streams, as shown by the presence of a synbranchid swamp eel, as well as erythrinid and non-ariid catfish specimens in several loci (*SI Appendix, SI Dataset 2*).

By *ca.* 110 ka, the sea had already retreated, as the marine fossils are reworked or oxidized in most trenches, in good agreement with the global eustatic history (Fig. 4D). The macrofossil content of the level topping the marine sequence, with only siliceous/phosphatic fossil remains of marine origin (*Discradisca* brachiopods and fish teeth), points to a differential preservation and a post-burial dissolution of calcareous specimens (including foraminifers) in marine deposits posteriorly pedogenetized. Phytoliths sampled in the very top of Unit A point to continental affinities, with the first conspicuous occurrence of grass phytoliths recorded in PN14 sample. The iron crust topping this unit at various loci further suggests intense surface weathering during a short time (Fig. 1). Afterwards, the Kourou sites registered a strong continental signature through pollen, phytoliths and charcoal, indicating extensive plain savanna to dry forest fringed conditions (Units B and C; Fig. 4B-C). The occurrence of natural (i.e., pre-human) fires is revealed by burnt phytoliths (*ca.* 28 %) and microcharcoals at KOU-AR6-06-PN15, and by macro-charcoals before 47 ka *cal* BP. This suggests that a dry interval may have occurred regionally, perhaps coinciding with a glacial interval (possibly MIS 4).

Charcoals suggest that tree diversity culminated *ca*. 47 ka cal BP, in the transition zone between a savanna and a coastal/swamp/riparian forest, or a mosaic of habitats including dryland forest. The presence of bootlace tree might attest to the presence of a

swamp forest in the surroundings by 43 ka *cal* BP, >100 km away from the coastline (Fig. 4B).

After a gap in the charcoal record, the 2-ka old level at KOU-AR6-04 yields clues of wet-plain and riparian habitats, with *Mabea* and hog plums. The latter tree, with edible fruits (mombin), might also be related to human occupation, documented in the area at that time (35). The youngest charcoal sample (*ca.* 800 *cal* BP) points to a swamp or riparian forest. The absence of phytolith and pollen record in Unit C impedes characterizing further the last pre-Columbian seasonally-flooded local savannas (34).

LIG marine communities from KOU-AR6: taxonomic diversity and ecological affinities

The estimated sea surface temperature for the Guiana Basin during the LIG was higher (28.9°C) than today [28.1°C (46)] (Fig. 4D). Warm periods (e.g., today and LIG) are characterized by an equatorial depletion of marine diversity, with diverse-most areas shifting towards higher latitudes, due to equatorial temperatures being higher than the physiological tolerance of certain species (11, 15, 16): brachyurans, bivalves and gastropods are particularly thermo-sensitive, and today their species diversity decreases in waters exceeding 20°C (17). To assess the diversity of KOU-AR6 metazoan paleocommunities by the warm LIG, we used a comprehensive survey performed in the 1950s for recent marine organisms of FG as a reference (45). We compared species and genus diversity against depth range and type of substrate (mud, muddy sands, dead shells, and sands), for corals, mollusks (gastropods, bivalves, and scaphopods), brachyuran decapods, echinoderms (sea stars and urchins), and bony fish. We chose this 1950s-survey as i) it is unparalleled as a sampling effort and ii) it was undertaken before the last decades' massive erosion of marine biodiversity of anthropogenic origin (47). As a result, only sea stars denote a lower cumulative diversity in the LIG than in recent samples of compatible substrates and wider bathymetric range (*SI Appendix*, Table S18). Despite a comparatively-limited sampling effort, further restricted by a *ca.* 5-m-deep depositional setting (unfavorable to the development of species-rich assemblages), corals, brachyurans, urchins, and bony fish have a similar alpha-diversity in the Kourou LIG samples and in recent samples, while KOU-AR6 mollusk alpha-diversity widely exceeds FG's recent one (twice to four times higher; *SI Appendix*, Table S18). This disparity in molluscan species richness may in part be due to the time-averaging of skeletonized components in death assemblages, accumulating over hundreds to thousands of years along the FG shoreline prior to anthropogenic impacts. Changing environmental factors allowed different species to inhabit these estuarine and coastal areas as time passed, with those death assemblages accumulating an ever-increasing species richness (48, 49).

Indeed, temperature does not explain the entire history of tropical marine diversity (14) and causes may be multiple for this coastal diversity drop between the LIG and the

1950s in FG, notably due to the large-scale marine retreat that occurred meanwhile and exhumed most of the Guianese continental shelf during the LGP (Fig. 4). At a shorter timescale, the shallow marine areas of FG have also experienced deep changes in terms of coastal environment and substrates over the last centuries, with mangroves and mudbanks—characterized by low taxonomic richness and high substrate homogeneity—spreading northwestward all over clear waters. This massive siltation is mainly due to the AP, a huge coastal flux of warm, hyposaline, nutrient-rich, and turbid surface-waters of Andean-Amazonian origin (24). This flow plays today a prominent role as a barrier between Brazil and the Caribbean for a wide array of marine animals, including reef fish and gastropods (25, 26). Indeed, its influence on biotic communities over the last interglacials is unknown (24–26). We used the recent geographic distribution of mollusk species recognized at KOU-AR6 as a proxy for testing the ecological affinities of this coastal Guianese fossil assemblage (*SI Appendix, SI Datasets 2–3*; Fig. 4). As a result, the closest relationships are retrieved between KOU-AR6 and recent mollusk communities from the Guianas, with 53 species in common. While these Guianese communities tightly group with a Southwestern and South Caribbean cluster, with Eastern Brazil as an offshoot (*SI Appendix*, Fig. S14), they have restricted affinities with the Amazon and Northeastern Brazil living communities. This somewhat contrasts with today's spatial pattern, where Guianese coastal communities are both impoverished and diverging taxonomically from the Caribbean ones, under the major influence of the AP (26). This result suggests that the spatial distribution of Western Atlantic tropical mollusks was not fully shaped by a barrier prefiguring the AP around LIG times, either related to salinity, turbidity, nutrient-balance, or temperature discrepancies. The virtual lack of fossil record documenting this penultimate warm period near the equator (Fig. 1A) impedes getting a broader picture on this very issue, but it clearly highlights where sampling efforts should increase in the future.

Inputs for conservation biology and perspectives for the near future

About 30 recent species, among foraminifers, cnidarians, sharks, bryozoans, brachiopods, and mollusks (14 species), have their first and/or earliest fossil record in LIG deposits at KOU-AR6 (*SI Dataset 2*), which significantly adds to their knowledge and may help for conservation policies (13). Most vertebrate taxa recognized in KOU-AR6 still inhabit FG seawater today, as endemic species of the Central-South American Atlantic coasts (e.g., *Isogomphodon oxyrhynchus, Carcharhinus porosus,* and *Sphyrna media*; *SI Appendix*, Tables S13–14). Due to overfishing, the sawfish, the smalltail, daggernose and scoophead sharks are critically endangered while the *Albula vulpes* bonefish is nearly threatened and the *Cynoscion acoupa* weakfish is vulnerable (*SI Dataset 2*). The presence of these species 125 ka ago in the same area and their current small range (*SI Dataset 2*) suggest low mobility on 10^5–10^6-year timescales, as predicted by spatial distribution models (13, 50). It would also be indicative of higher vulnerability to overfishing than to warming for

these taxa (15–17). As such, this study on past communities may open new perspectives regarding in-depth taxonomic studies, community ecology analyses, and extinction risks of the considered assemblages. Hopefully, new records would follow and help bridging stratigraphic and biogeographic gaps on a regional scale (14).

Environmental conditions during the climax of MIS 5e strikingly echo the most pessimistic scenarios for global warming and sea-level rise in 2100 AD, notably in Central and South America (46, 51). This analogy has a particular resonance, as the Guianese coastal areas located at less than 10 m above modern sea-level are critically concerned by the current sea-level and temperature rises and subsequent cascading risks, such as vector-borne disease epidemics, and drastic changes in Amazon biome dynamics (51–53). Indeed, low-elevation coastal zones hosting around 20, 55 and 80 % of FG, Guyana, and Suriname inhabitants, respectively, are at risk of being entirely flooded before 2100 AD (51, 54, 55), as are irremovable infrastructures of the area (e.g., airports and Europe's Spaceport). As the future may be learnt from the past in terms of marine biodiversity and coastal ecosystem dynamics and fate (16, 47, 56), we hope that the present work would help raise collective awareness of the major environmental upheavals that the region may experience in the next century, especially for decision-makers, whether local or transnational.

Material and Methods

The material was collected through handpicking (charcoals) and screen-washing of more than one metric ton of sediments [with 2 mm, 1 mm, 0.7 mm meshes for most fossil groups, and smaller meshes for microvertebrates (0.4 mm) and foraminifers (150 and 63 µm)]. The fossil specimens belong to the collections of the *Université de Guyane*, in Cayenne. When large numbers of specimens were available for a given species, other specimens have been further stored in the collections of the *Université de Montpellier*.

Age constraints were provided through U-Th datings on corals (Unit A), optically-stimulated luminescence (OSL) dating on quartz grains (Units A and B) and ^{14}C datings (Unit C).

Taxonomic identifications were undertaken by recognized specialists of each group of interest, aiming at retaining the most accurate and conservative assignment level. These assignments range from species to family level, highly depending on completeness of the concerned KOU-AR6 records and/or on current knowledge discrepancies about recent taxa themselves (*SI Appendix*, Tables S7–17).

For comparing the diversity of KOU-AR6 past communities (five marine samples over a 0.5 km^2 surface at a *ca*. 5-m depth; this work), we used a comprehensive survey (45)

performed in 1954–1957 on recent marine organisms on the Guianese Continental Plate (400 samples over *ca*. 40,000 km^2, including 110 samples for a 0–29-m depth range and 272 for a 20–49-m depth range) on compatible substrates and a wider bathymetric range (mud, 0–30-m depth; muddy sands, dead shells, and sands, 20–49-m depth).

To define the ecological affinities of KOU-AR6 LIG mollusks at the Western Atlantic scale, a taxon/area matrix, widely inspired from that of a recent biogeographic analysis (26), was built for the 74 species having a well-defined distribution area today (*SI Appendix, SI Datasets 2–3*). For that, we used the mapper tool of the Ocean Biodiversity Information System repository (https://mapper.obis.org), completed by an atlas of French Guiana's mollusks (57). We then ran UPGMA and parsimony analyses with PAUP* 4.0a.169 (58).

Acknowledgments

This article is dedicated to the memory of François Catzeflis, as a scientist and a human, for his major contribution to evolutionary biology in FG, and for having inspired us in our long quest for Guianese fossils. We are grateful to Nils Stenseth (invited editor), but also to Moriaki Yasuhara and an anonymous reviewer for their constructive and stimulating remarks on previous versions of the manuscript. We are deeply indebted to Martijn van den Bel and everybody at INRAP in Cayenne-Matoury for granting access to their facilities in 2018, to Michel Brossard, Michel Macarit and Lionel Hautier for their participation to field and screen-washing operations, to Carlos Jaramillo for preparing early samples and for fruitful discussion, and to Henry Hooghiemstra for providing relevant suggestions on our manuscript. We are particularly thankful to the *Centre National d'Etudes Spatiales* (Sandrine Richard and Henri Brunet-Lavigne), the *Centre Spatial Guyanais*, Eiffage (Henri Beny) and Sodexo (Patrick Raverat). This work was funded by the French *Agence Nationale de la Recherche* (ANR) in the framework of both the LabEx CEBA (ANR-10-LABX-25-01), through the projects Source, NeotroPhyl, Timespan and Emergence, and the GAARAnti project (ANR-17-CE31-0009). OA acknowledges funding from the Brazilian Council of Science and Technological Development (CNPq 304693/2021-9). NHW acknowledges CNHM/funding from the European Research Council (ERC 2019 StG 853394). RJB acknowledges funding from the Australian Research Council (ARC DP220100195 and LE200100022). PGV acknowledges funding from the French ANR-PIA program (ANR-18-MPGA-0006). This is ISEM-Sud article n°2024-051.

References

1. H.P. Comes, J.W. Kadereit, The effect of Quaternary climatic changes on plant distribution and evolution. *Trends Plant Sci.* **3**, 432–438 (1998).

2. M. Dynesius, R. Jansson, Evolutionary consequences of changes in species' geographical distributions driven by Milankovitch climate oscillations. *Proc. Natl. Acad. Sci. U.S.A.* **97**, 9115–9120 (2000).

3. W.B. Ludt, L.A. Rocha, Shifting seas: the impacts of Pleistocene sea-level fluctuations on the evolution of tropical marine taxa. *J. Biogeogr*. **42**, 25–38 (2015).

4. L.B. Railsback *et al.*, An optimized scheme of lettered marine isotope substages for the last 1.0 million years, and the climatostratigraphic nature of isotope stages and substages. *Quat. Sci. Rev.* **111**, 94–106 (2015).

5. R.M. Spratt, L.E. Lisiecki, A Late Pleistocene sea level stack. *Clim. Past* **12**, 1079–1092 (2016).

6. P. Giresse *et al.*, Beachrocks of the last low sea level, substrate of the Great Amazon Reef system along the outer Guiana shelf. *Geo-Marine Lett.* **43**, 10 (2023).

7. A. Dutton, K. Lambeck, Ice volume and sea level during the last interglacial. *Science* **337**, 216–219 (2012).

8. A. Rovere *et al*., The analysis of Last Interglacial (MIS 5e) relative sea-level indicators: Reconstructing sea-level in a warmer world. *Earth-Sci. Rev.* **159**, 404–427 (2016).

9. P.L. Gibbard, M.J. Head, The Quaternary period. In Geologic Time Scale 2020, F.M. Gradstein, J.G. Ogg, M.D. Schmitz, G.M. Ogg (eds.), Elsevier, pp. 1217–1255 (2020).

10. K. Rubio-Sandoval, et al., A review of last interglacial sea-level proxies in the western Atlantic and southwestern Caribbean, from Brazil to Honduras. *Earth Syst. Sci. Data* **13**, 4819–4845 (2021).

11. W. Kiessling *et al.*, Equatorial decline of reef corals during the last Pleistocene interglacial. *Proc. Natl. Acad. Sci. U.S.A.* **109**, 21378–21383 (2012).

12. A. Rovere *et al*., The World Atlas of Last Interglacial Shorelines (version 1.0). *Earth Syst. Sci. Data* **15**, 1–23 (2023).

13. S. Finnegan *et al.*, Using the fossil record to understand extinction risk and inform marine conservation in a changing world. *Ann. Rev. Marine Sci.* **16,** 1–27 (2023).

14. M. Yasuhara *et al*., Hotspots of Cenozoic tropical marine biodiversity. *Oceanogr. Mar. Biol.* **60**, 243–300 (2022).

15. O. Rama-Corredor *et al.*, Parallelisms between sea surface temperature changes in the western tropical Atlantic (Guiana Basin) and high latitude climate signals over the last 140 000 years. *Clim. Past* **11**, 1297–1311 (2015).

16. M. Yasuhara *et al.*, Past and future decline of tropical pelagic biodiversity. *Proc. Natl. Acad. Sci. U.S.A.* **117**, 12891–12896 (2020).

17. M. Yasuhara, C.A. Deutsch, Paleobiology provides glimpses of future ocean: Fossil records from tropical oceans predict biodiversity loss in a warmer world. *Science* **375**, 25–26 (2022).

18. J. Boggan *et al.*, *Checklist of the plants of the Guianas (2nd Edition)*, Smithsonian's Biological Diversity of the Guianas Program series 30 (1997).

19. L.-F. Artigas *et al*., Marine biodiversity in French Guiana: estuarine, coastal, and shelf ecosystems under the influence of Amazonian waters. *Gayana* **67**, 302–326 (2003).

20. A. Sánchez Meseguer *et al.*, Diversification dynamics in the Neotropics through time, clades, and biogeographic regions. *Elife* **11**, e74503 (2022).

21. A.K. Gibbs, C.N. Barron, F. Tabeart, The geology of the Guiana Shield (Vol. 246), New York: Oxford University Press (1993).

22. P.-O. Antoine *et al.*, Un inventaire fossile de la Guyane : historique et nouvelles perspectives. *Géologues* **206**, 28–30 (2020).

23. J.C. Lindeman, The vegetation of the Coastal Region of Suriname. Results of the scientific expedition to Suriname 1948—49 botanical series No. 1. *Meded. Bot. Mus. Herb. Rijks Univ. Utrecht* **113**, 1–135 (1952).

24. M. Pujos, J.-M. Froidefond, Water masses and suspended matter circulation on the French Guiana continental shelf. *Contin. Shelf Res*. **15**, 1157–1171 (1995).

25. S.R. Floeter *et al.*, Atlantic reef fish biogeography and evolution. *J. Biogeogr.* **35**, 22–47 (2008).

26. E. Giachini Tosetto, A. Bertrand, S. Neumann-Leitão, M. Nogueira Júnior, The Amazon River plume, a barrier to animal dispersal in the Western Tropical Atlantic. *Scientific Reports* **12**, 537 (2022).

27. M. Mestre, S. Delpech, "Plateau des Mines", Saint-Laurent du Maroni. Excavation report, INRAP, Cayenne (2008).

28. G. Odonne *et al.*, Long-term influence of early human occupations on current forests of the Guiana Shield. *Ecology* **100**, e02806 (2019).

29. M.G. Plew, L. Daggers, *The Archaeology of Guyana (2nd Edition)*, (University of Guyana Press, 2022).

30. E. Palvadeau, *Géodynamique quaternaire de la Guyane Française*. BRGM, Université de Bretagne Occidentale, 255 p. (1999).

31. G. Brunier *et al*. Evolution of the French Guiana coast from Late Pleistocene to Holocene based on chenier and beach sand dating. *Region. Envir. Change* **22**, 122 (2022).

32. P.U. Clark *et al.*, The last glacial maximum. *Science* **325**, 710e714 (2009).

33. C. J. Van Meerbeeck, H. Renssen, D. M. Roche, How did Marine Isotope Stage 3 and Last Glacial Maximum climates differ? – Perspectives from equilibrium simulations. *Clim. Past* **5**, 33–51 (2009).

34. J. Iriarte *et al.*, Fire-free land use in pre-1492 Amazonian savannas. *Proc. Natl. Acad. Sci. U.S.A.* **109**, 6473–6478 (2012).

35. M.M. van den Bel, Nouveaux apports sur l'archéologie du littoral de Guyane : de la préhistoire à la conquête. *J. Soc. Américanistes* **104**-2 (2018).

36. N. Sariaslan, M.R. Langer, Atypical, high-diversity assemblages of foraminifera in a mangrove estuary in northern Brazil. *Biogeosci*. **18**, 1–18 (2021).

37. A.C.S. Almeida, F.B.C. Souza, L.M. Vieira, Malacostegine bryozoans (Bryozoa: Cheilostomata) from Bahia State, northeast Brazil: taxonomy and non-indigenous species. *Marine Biodiv.* **48**, 1463–1488 (2017).

38. L.M. Vieira, A.E. Migotto, J.E. Winston, Synopsis and annotated checklist of Recent marine Bryozoa from Brazil. *Zootaxa* **1810**, 1–39 (2008).

39. D.J. Hughes, J.B.C. Jackson, Do constant environments promote complexity of form?: The distribution of bryozoan polymorphism as a test of hypotheses. *Evolution* **44**, 889–905 (1990).

40. T. Van der Hammen, A palynological study on the Quaternary of British Guiana. *Leidse Geol. Meded*. **29**: 125–180 (1963).

41. D. R. Piperno, *Phytoliths: a comprehensive guide for archaeologists and paleoecologists*, (Rowman Altamira, 2006).

42. C. Crifò, C.A. Strömberg, Small-scale spatial resolution of the soil phytolith record in a rainforest and a dry forest in Costa Rica: applications to the deep-time fossil phytolith record. *Palaeogeogr., Palaeoclimatol., Palaeoecol.* **537**, 109107 (2020).

43. J. Iriarte *et al.*, Late Holocene Neotropical agricultural landscapes: phytolith and stable carbon isotope analysis of raised fields from French Guianan coastal savannahs. *J. Archaeol. Sci.* **37**, 2984–2994 (2010).

44. S. Guitet, R. Pélissier, O. Brunaux, G. Jaouen, D. Sabatier, Geomorphological landscape features explain floristic patterns in French Guiana rainforest. *Biodiv. Conserv.* **24**, 1215–1237 (2015).

45. J. Durand, Notes sur le plateau continental guyanais : les éléments principaux de la faune et leurs relations avec le fond. *Cah. ORSTOM* **3**, 1–99 (1959).

46. J.B.C. Jackson *et al.*, Historical overfishing and the recent collapse of coastal ecosystems. *Science* **293**, 629–637 (2001).

47. C. Chaudhary *et al*., Global warming is causing a more pronounced dip in marine species richness around the equator. *Proc. Natl. Acad. Sci. U.S.A.* **118**, 1–6 (2021).

48. G.M. Staff, E.N. Powell, The paleoecological significance of diversity: the effect of time averaging and differential preservation on macroinvertebrate species richness in death assemblages. *Palaeogeogr., Palaeoclimatol., Palaeoecol*. **63**, 73–89 (2008).

49. A. Tomašových, S.M. Kidwell, Fidelity of variation in species composition and diversity partitioning by death assemblages: time-averaging transfers diversity from beta to alpha levels. *Paleobiol*. **35**, 94–118 (2009).

50. C.J. Reddin *et al.,* Victims of ancient hyperthermal events herald the fates of marine clades and traits under global warming. *Global Change Biology* **27**, 868–878 (2021).

51. I. Hagen *et al*., Climate change-related risks and adaptation potential in Central and South America during the 21st century. *Environ. Res. Lett.* **17**, 033002 (2022).

52. J. Barlow *et al.*, The future of hyperdiverse tropical ecosystems. *Nature* **559**, 517–526 (2018).

53. B. Neumann, A.T. Vafeidis, J. Zimmermann, R.J. Nicholls, Future coastal population growth and exposure to sea-level rise and coastal flooding-a global assessment. *PLoS ONE* **10**, e0118571 (2015).

54. A. Heuret, S. Bodin, L. Marivaux, P.-O. Antoine, Des étoiles aux fossiles. Quand Ariane 6 dévoile la Guyane pléistocène. *Une saison en Guyane* **7**, 4–9 (2021).

55. G. McGranahan, D. Balk, B. Anderson, The rising tide: assessing the risks of climate change and human settlements in low elevation coastal zones. *Environ. Urban.* **19**, 17–37 (2007).

56. H.K. Lotze, L. McClenachan, Marine historical ecology: Informing the future by learning from the past. In *Marine Community Ecology and Conservation*, M.D. Bertness et al. (eds). Sunderland: Sinauer Associates, Inc., 165-200 (2014).

57. D. Massemin, D. Lamy, J.-P. Pointier, O. Gargominy, Coquillages et escargots de Guyane. *Publications Scientifiques du Muséum*, MNHN, Paris (2009).

58. D. Swofford, PAUP* 4.0a.169: phylogenetic analysis using parsimony (2021).

59. The Paleobiology Database. http://paleobiodb.org/data1.2/occs/list_doc.html. Accessed on 2023-11-29 at 16:20:31 GMT.

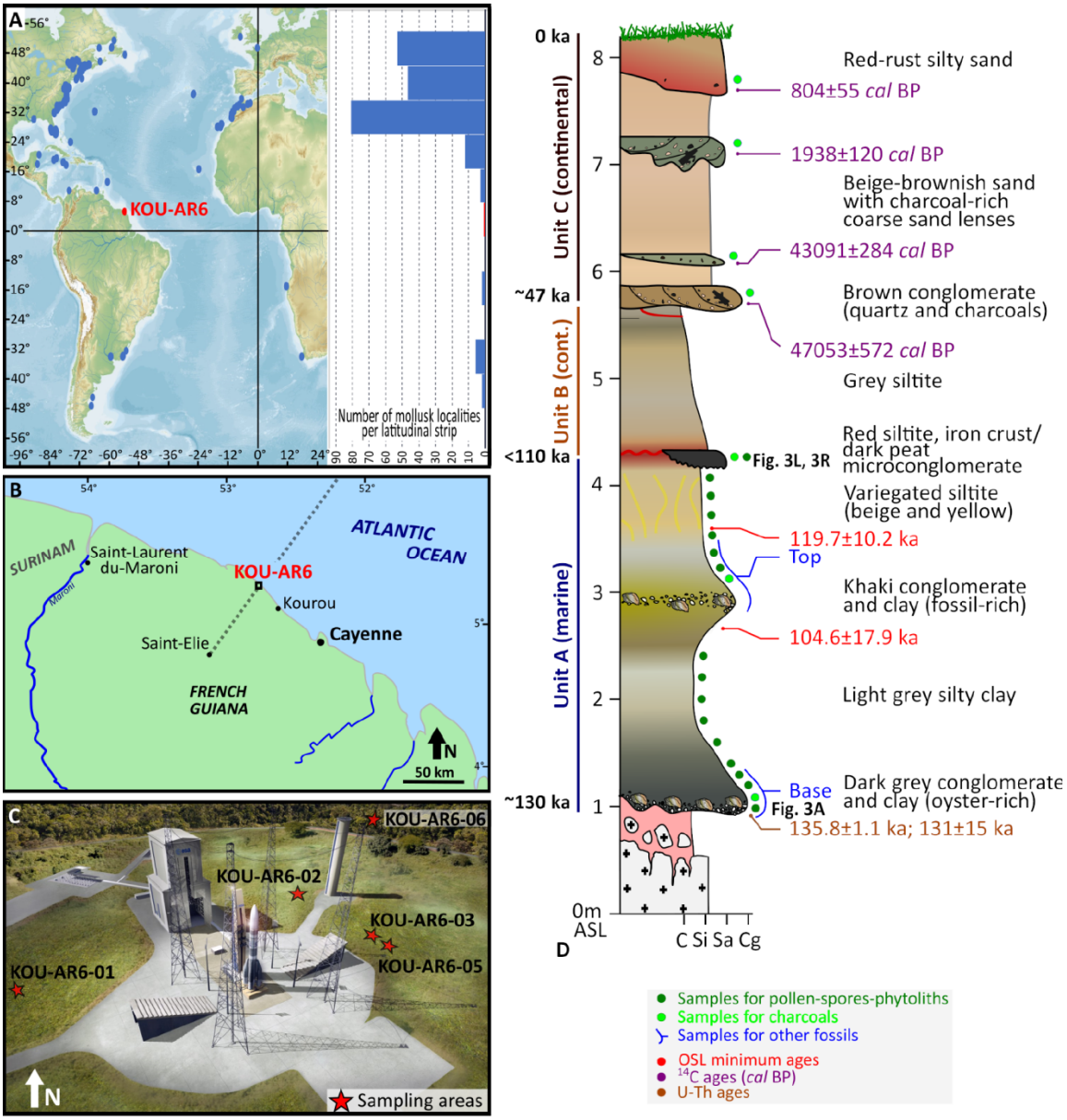

Figure 1. Location map *(A)* of the Middle and Late Pleistocene marine mollusk localities, between 60°S and 60°N in the Atlantic Ocean (see *SI Dataset 1*), as retrieved in the Paleobiology Database (59), and of the Pleistocene–Holocene KOU-AR6 sections and sampling sites *(B–C)*, by the Ariane 6 launcher pad (KOU-AR6-01 to -06). The dashed line denotes the cross sections as seen in figure 4. Composite stratigraphic section *(D)* at Kourou, French Guiana, with sedimentological descriptions and multi-proxy age constraints. Sampling levels are approximate (for detailed information on each section and sampling efforts, see *SI Appendix*, Fig. S11). ASL, Above Sea-Level; BP, Before Present; C, clay; *cal*, calibrated; Cg, conglomerate; cont., continental; Sa, sand; Si, siltite.

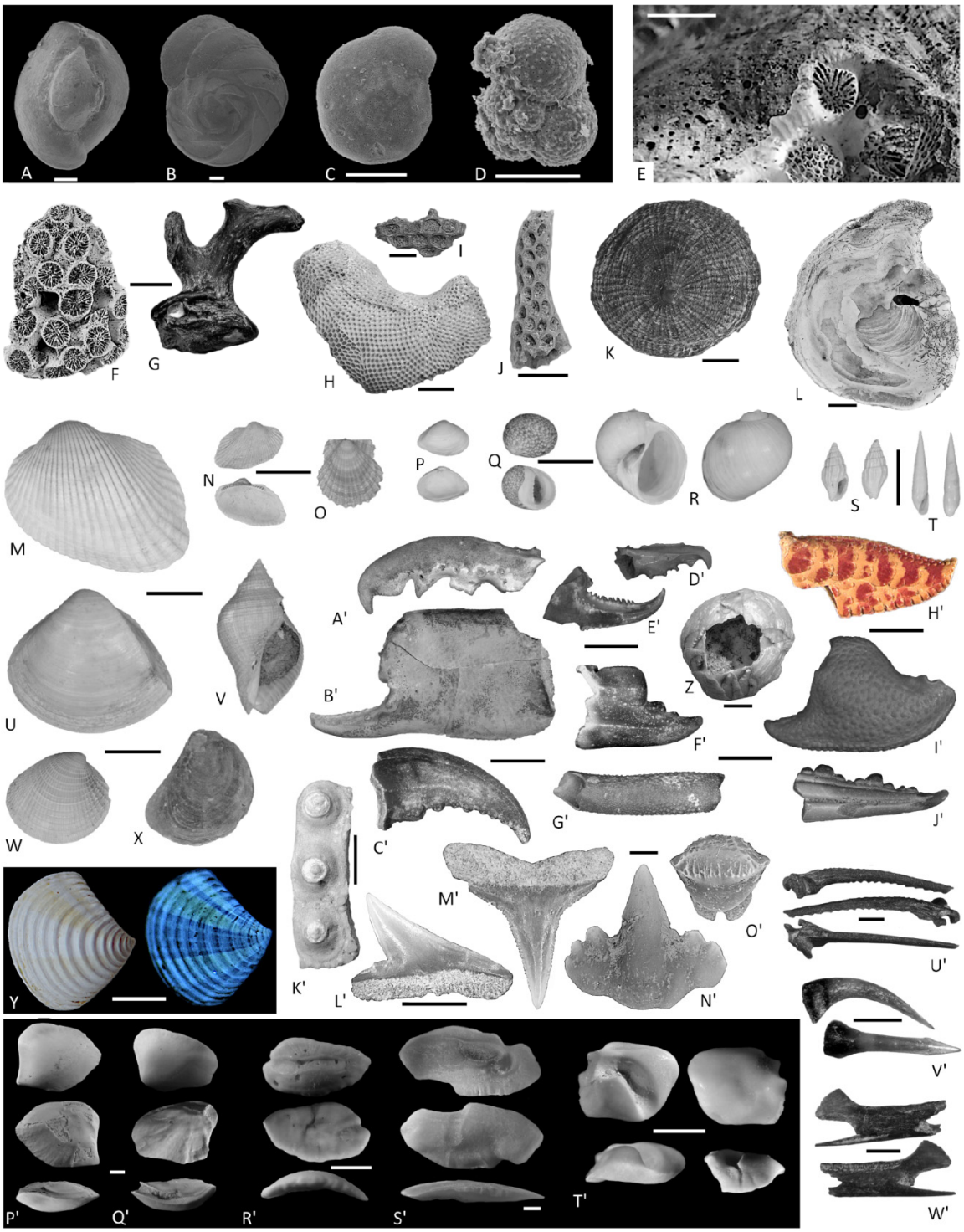

Figure 2. Marine foraminifer and metazoan communities from Unit A (~130–115 ka, Last Interglacial) and associated taxa in KOU-AR6 sections, Kourou, French Guiana. Foraminifers (A-D). *(A) Quinqueloculina seminula* (KOU-AR6-05 top); *(B) Eponides repandus* (KOU-AR6-03 base); *(C) Ammonia veneta* (KOU-AR6-03 base); *(D) Globigerina bulloides* (KOU-AR6-05 top); (*E*) Detail of an oyster shell, encrusted by bryozoans and a small colony of *Astrangia rathbuni* corals and perforated by *Entobia* sponge boreholes (KOU-AR6-03 base). Cnidarians (F, G). *(F) Astrangia rathbuni*, colony (KOU-AR6-06 base);

(G) Pacifigorgia sp., basal portion (KOU-AR6-06 base, 2 mm). Bryozoans (H–J). *(H) Biflustra arborescens* (KOU-AR6-01); *(I) Steginoporella magnilabris* (KOU-AR6-03 top); *(J) Conopeum loki* (KOU-AR6-05 top). *(K)* Brachiopods, *Discradisca antillarum,* in external view (KOU-AR6-06 top). Mollusks (L – Z). *(L) Crassostrea* sp., flat (right) valve in inner view, perforated by pholadid bivalves and *Entobia* (KOU-AR6-02). Mollusca (M-X). *(M) Lunarca ovalis* (KOU-AR6-05); *(N) Sheldonella bisulcata* (KOU-AR6-05); *(O) Leptopecten bavayi* (KOU-AR6-05); *(P) Caryocorbula contracta* (KOU-AR6-05); *(Q) Vitta virginea* (KOU-AR6-05); *(R) Stigmaulax cayennensis* (KOU-AR6-05); *(S) Costoanachis avara* (KOU-AR6-03); *(T) Eulima bifasciata* (KOU-AR6-03); *(U) Mulinia cleryana* (KOU-AR6-05); *(V) Stramonita haemastoma* (KOU-AR6-05); *(W) Chione cancellata* (KOU-AR6-05); *(X) Crassostrea rhizophorae* (KOU-AR6-03); *(Y) Crassinella lunulata*, under natural light (left) and 395-nm wavelength UV light (right). Crustaceans. *(Z)* Balanomorphs: *Amphibalanus* sp., individual with articulated wall plates (KOU-AR6-01). Axiidean (A'–B'), anomuran (E'–F'), and brachyuran decapods (G'–H'). *Neocallichirus* sp., left cheliped dactyl, outer margin *(A')* and left cheliped propodus, outer margin *(B')*. Callichiridae indet., left cheliped dactyl, inner margin *C')* and left cheliped pollex, outer margin *(D')*. *Pachycheles* sp., left cheliped, outer margin, showing the palm and pollex *(E')*. *Petrolisthes* sp., pollex of right cheliped, outer margin view *(F')*. Eriphioidea (*Eriphia*/*Menippe*), dactyl of right cheliped, inner margin view *(G')* and distalmost part of pollex of right cheliped *(H')*. ?*Persephona* sp., merus of cheliped indet *(I')*. Portunidae indet., fragment of cheliped pollex *(J')*. Echinoderms. *(K') Arbacia punctulata* (KOU-AR6-06 Base), test fragment. Elasmobranchs (L'–O'). *(L') Isogomphodon oxyrhynchus* (upper tooth); *(M') Rhizoprionodon* sp. (lower lateral tooth); *(N') Ginglymostoma cirratum* (lower tooth); *(O') Hypanus* sp. Bony fish otoliths in rotate views (P'–T'). *(P') Aspistor luniscutis* (KOU-AR6-05 Top); *(Q') Cathorops spixii* (KOU-AR6-05 Top); *(R') Thalassophryne* sp. (KOU-AR6-03 Base); *(S') Macrodon ancylodon* (KOU-AR6-03 Base); *(T') Stellifer rastrifer* (KOU-AR6-05 Top). Bony fish teeth and bones (U'–W'). *(U')* Erythrinidae indet., tooth (KOU-AR6-03 Base); *(V')* unidentified freshwater siluriform, pectoral spine (KOU-AR6-03 Base); *(W')* Nettastomatidae indet., dentary (KOU-AR6-03 Base). Scalebars = 100µm (A–D), 5 mm (E, F, Y, A'–D', G'–I', M'), 2 mm (G, H, F', J', V'), 1 mm (I–K, Z, E', K', L', N'–Q', R'–U', W'), 10 mm (L–X).

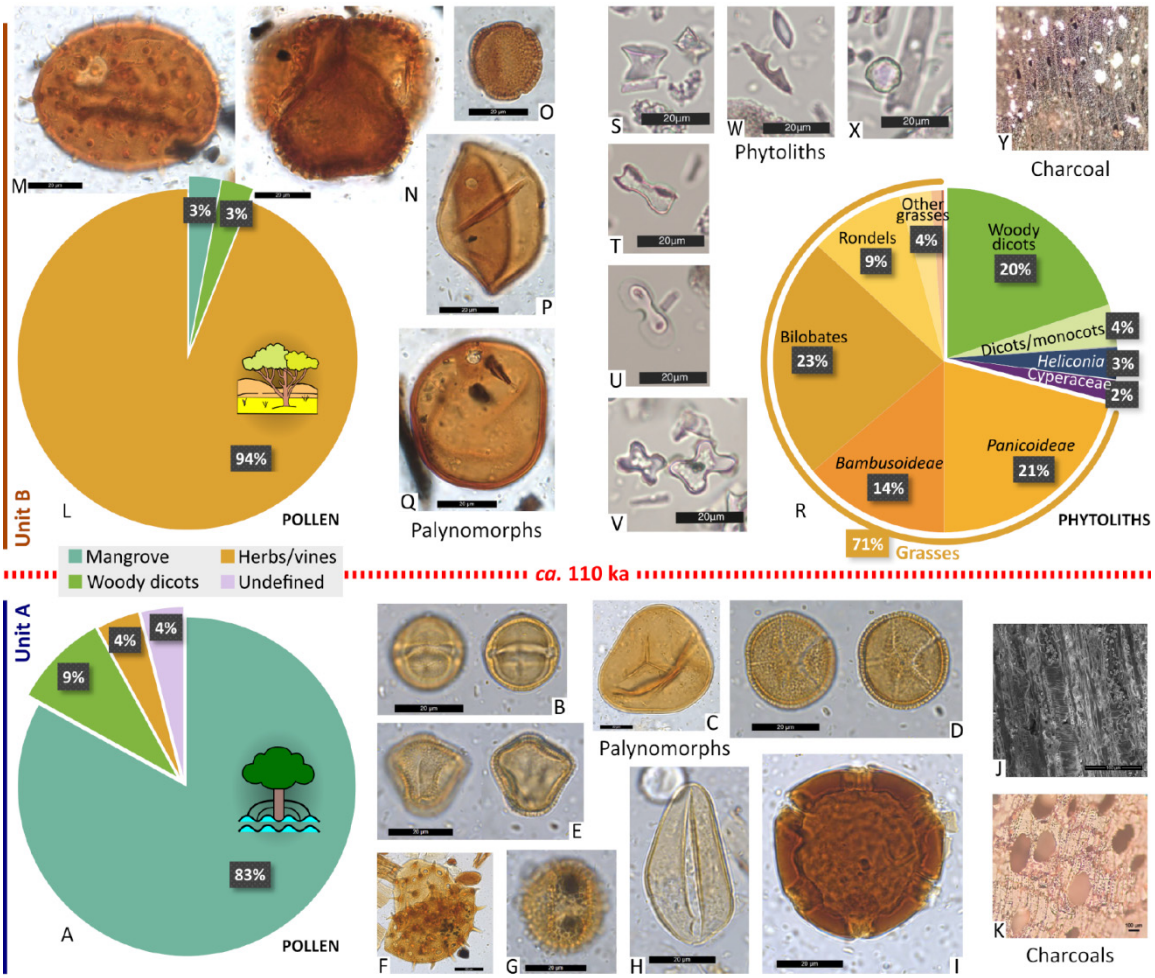

Figure 3. Pollen and phytolith assemblages and charcoal fragments from Unit A (*ca.* 130–115 ka, Last Interglacial; A–K) and Unit B (Last Glacial Period (*ca.* 110–*ca.* 50 ka; L–Y) in KOU-AR6 sections, Kourou, French Guiana. *(A)* Pollen diagram of Unit A (KOU-AR6-PN9), with typical palynomorphs (B–I) and charcoals (J, K); *(B) Rhizophora* sp., red mangrove; *(C) Acrostichum* sp., mangrove fern; *(D) Hedyosmum* sp.; *(E) Schefflera* sp.; *(F) Peltaea* sp.; *(G) Ilex* sp.; *(H) Attalea* type; *(I) Symphonia* sp.; *(J)* cf. *Rhizophora*; *(K)* Chrysobalanaceae. *(L)* Pollen diagram of Unit B (KOU-AR6-PN15), with typical palynomorphs (M–Q); *(M) Mauritia* sp.; *(N) Schultesia* sp.; *(O)* Rubiaceae indet.; *(P)* Poaceae indet.; *(Q)* Poaceae indet.; *(R)* Phytolith diagram of Unit B with typical phytoliths (KOU-AR6-PN15; S–X) and charcoal (KOU-AR04 Base; Y); *(S)* Poaceae, rondel; *(T)* Poaceae, bilobate; *(U)* Poaceae, *Bambusoideae*; *(V)* Poaceae, *Panicoideae*; *(W)* Zingiberales, *Heliconia*; *(X)* Woody dicot; *(Y)* cf. Myrtaceae (charcoal). Scalebars = 20 µm (B–E, G, H, M–Q, S–X), 50 µm (F), or 100 µm (J, K, Y).

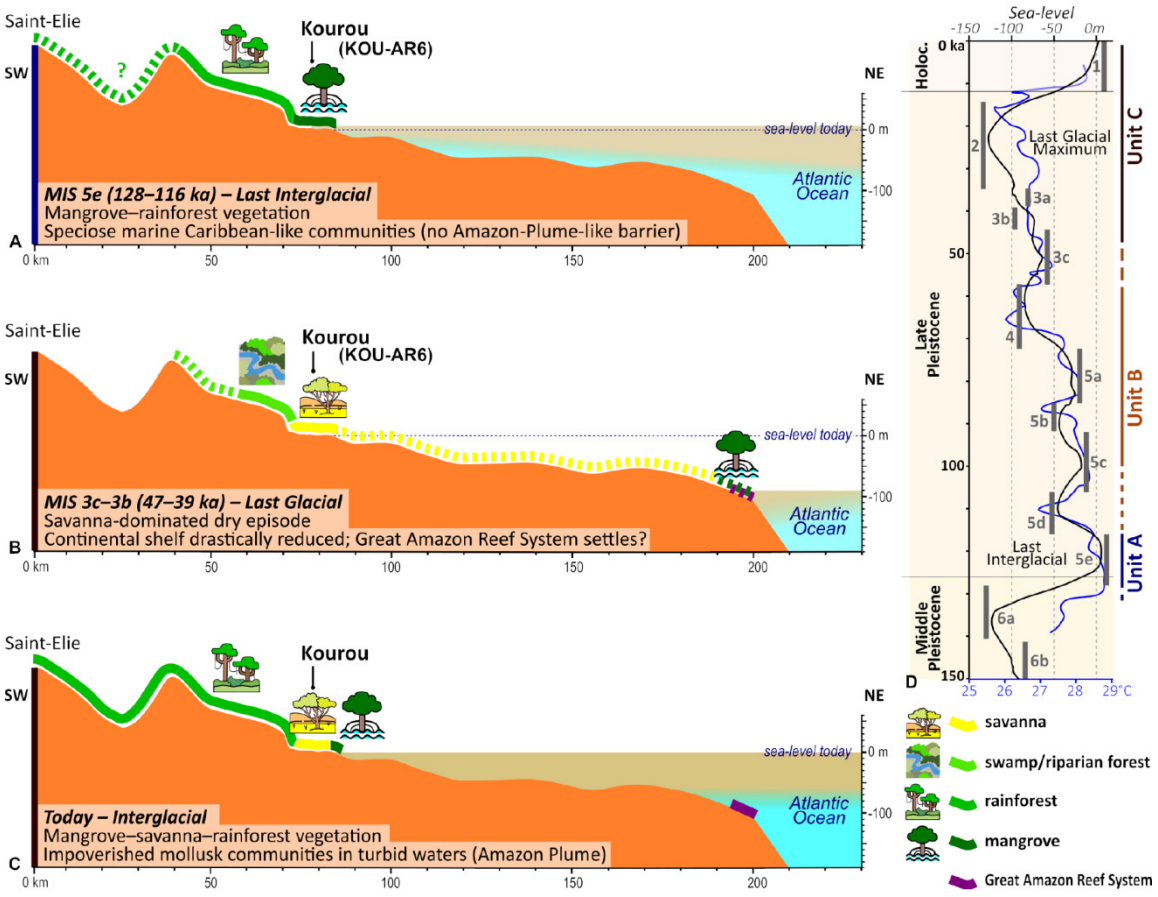

Figure 4. Hypothesized evolution of Late Pleistocene–Holocene landscapes in French Guiana, using fossil proxies, sedimentary facies and radioisotopic age constraints available at KOU-AR6 sections, Kourou. *(A)* during MIS 5e (*ca.* 130–115 ka; Unit A, marine and mangrove settings). *(B)* during MIS 3c–3b (47–39 ka; Unit C, base; continental settings). *(C)* today (Unit C, top, coastal-continental settings). Although documenting fires at its base, Unit B was not sufficiently time-constrained to be satisfactorily depicted here. The presence of a mangrove landscape bordering the Great Amazon Reef System (GARS) at 47–39 ka is hypothetical. Main environmental and ecological features related to the sea-level changes, observed locally/regionally over the last climatic cycle, are summarized in the boxes in *A–C*. *(D)* sea-level curve and marine isotopic stages, modified from Railsback *et al.* (4) and Gibbard and Head (9); sea-surface temperatures modified from Rama-Corredor *et al.* (46). Location of the GARS from Giresse *et al.* (6). For further details regarding age constraints, sampling sections, fossil content, biogeographic/ecological affinities, and corresponding levels, see *SI Appendix, SI Datasets 1–3*.

Table 1. Taxonomic diversity of marine and continental communities from the KOU-AR6 Pleistocene–Holocene sections, Kourou, French Guiana.

Higher taxa	MARINE Unit A ca. 130–115 ka	CONTINENTAL Unit B ca. 110 ka–ca. 50 ka	Unit C 47–1 ka	Total (distinct taxa)
Foraminifera (foraminiferans)	12	-	-	12
Porifera (sponges)	1	-	-	1
Cnidaria (corals, gorgons)	2	-	-	2
Bryozoa (bryozoans)	19	-	-	19
Annelida (serpulid worms)	1	-	-	1
Mollusca (mollusks)	87	-	-	87
Scaphopoda (scaphopods)	2	-	-	-
Bivalvia (bivalves)	35	-	-	-
Gasteropoda (gastropods)	50	-	-	-
Brachiopoda (brachiopods)	1	-	-	1
Arthropoda (arthropods)	13	-	-	13
Cirripedia (cirripeds)	2	-	-	-
Decapoda (decapods)	11	-	-	-
Echinodermata (echinoderms)	3	-	-	3
Echinoidea (urchins)	2	-	-	-
Asteroidea (sea stars)	1	-	-	-
Vertebrata (vertebrates)	46	-	-	46
Elasmobranchii (rays, sharks)	11	-	-	-
Actinopterygii (ray-finned fishes)	35	-	-	-
Plantae (plants)	41	35	22	92
Charcoal	10	8	22	-
Phytoliths	2	18	-	-
Pollen	30	11	-	-
TOTAL per Unit	226	35	22	277

Some plant taxa have been recognized from charcoal and/or pollen in the same unit or in distinct units, hence distinct figures in the last line (distinct taxa per Unit) and the last column (distinct taxa identified at KOU-AR6, regardless of the yielding Unit).

Supplementary Information Appendix

A Late Pleistocene coastal ecosystem in French Guiana was hyperdiverse relative to today

Pierre-Olivier Antoine, Linde Wieringa, Sylvain Adnet, Orangel Aguilera, Stéphanie Bodin, Stephen Cairns, Carlos A. Conejeros-Vargas, Jean-Jacques Cornée, Žilvinas Ežerinskis, Jan Fietzke, Natacha O. Gribenski, Sandrine Grouard, Austin Hendy, Carina Hoorn, Renaud Joannes-Boyau, Martin R. Langer, Javier Luque, Laurent Marivaux, Pierre Moissette, Kees Nooren, Frédéric Quillévéré, Justina Šapolaitė, Matteo Sciumbata, Pierre G. Valla, P., Nina H. Witteveen, Alexandre Casanova, Simon Clavier, Philibert Bidgrain, Marjorie Gallay, Mathieu Rhoné & Arnauld Heuret

1. Material

The fossil material belongs to the collection of the Université de Guyane, France. Whenever possible, i.e., if large numbers of specimens are available for a given species, a part of the collection is further stored in the collections of the Université de Montpellier, France.

1.1. Sampling localities

Table S1: Sampling localities in Pleistocene–Holocene sections around the ELA4 Ariane 6 launcher pad, Kourou, French Guiana. ASL, above sea-level.

Name	*Latitude (N)*	*Longitude (W)*	*Height (top)*	*Sampling date*	*Sampled for*
KOU-AR6-01	5°15.878’	52°47.650’	6 m ASL	February 14, 2019	Macrofossils
KOU-AR6-02	5°15.957’	52°47.496’	6 m ASL	February 14, 2019	Macrofossils
KOU-AR6-03	5°15.893’	52°47.455’	6 m ASL	April 8, 2019	Macrofossils, Microfossils, Pollen, U-series dating
KOU-AR6-04	5°15.739’	52°47.404’	9 m ASL	April 9, 2019	Charcoal, ^{14}C dating
KOU-AR6-05	5°15.901’	52°47.463’	6 m ASL	April 11, 2019	Macrofossils, Microfossils
KOU-AR6-06	5°16.135’	52°47.324’	4 m ASL	October 7, 2021	Macrofossils, Microfossils, Pollen-phytoliths, U-Th dating, OSL dating

KOU-AR6-01 locality

Fig. S1. Trench KOU-AR6-01, with giant exhaust-aimed and gantry infrastructures for Ariane 6 in the background (top left and right, respectively). Water fills the bottom of the stratigraphic sequence, thus covering the basal oyster-rich conglomerate and grey clays, being sampled by the excavator bucket. Photograph by A.H.

Nature: trench
Investigated in: February 14, 2019
Access: excavated and filled up immediately
Amount of sediment sampled: unknown (>100 kg), in basal oyster-rich conglomerates and grey clays
Handpicking: yes
Screenwashing: yes

KOU-AR6-02 locality

***Fig. S2*.** Trench KOU-AR6-02. The complete sequence is visible. Photograph by A.H.

Nature: trench
Investigated in: February 14, 2019
Access: excavated and filled up immediately
Amount of sediment sampled: unknown (>100 kg), in basal oyster-rich conglomerates and grey clays
Handpicking: yes
Screenwashing: yes

KOU-AR6-03 locality

***Fig. S3*.** Trench KOU-AR6-03. The complete sequence is visible, starting from the top of pink saprolites (bottom) overlaid by basal oyster-rich conglomerate and grey clays. Photograph by P.-O.A.

Nature: trench
Investigated in: April 8, 2019
Access: excavated and filled up immediately
Amount of sediment sampled: 320 kg in basal conglomerates and grey clays (Base); 30 kg in kaki conglomerate and clays (Top)
Handpicking: yes
Screenwashing: yes
Sampled for: Macrofossils, Microfossils, Pollen, U-Th dating

KOU-AR6-04 locality

Fig. S4. Ditch KOU-AR6-04 (detail). Only the topping sequence, of continental origin, is accessible. Note the presence of in-situ charcoals. Photograph by P.-O.A.

Nature: ditch
Investigated in: April 9, 2019
Access: accessible
Amount of sediment sampled: N/A
Handpicking: yes (tree stumps and loose charcoals)
Screenwashing: No
Sampled for: Charcoal, ^{14}C dating

KOU-AR6-05 locality

***Fig. S5*.** Trench KOU-AR6-05, with the Ariane 6 rocket gantry in the background (left). The complete stratigraphic sequence is visible, starting by the basal oyster-rich conglomerate and grey clays. Photograph by P.-O.A.

Nature: trench
Investigated in: April 11, 2019
Access: excavated and filled up immediately
Amount of sediment sampled: 150 kg in kaki conglomerate and clays (Top)
Handpicking: yes
Screenwashing: yes
Sampled for: Macrofossils, Microfossils

KOU-AR6-06 locality

***Fig. S6*.** Trench KOU-AR6-06. To the left, sampling for OSL-dating (OSL-1). On the right side of the trench, sampling for pollen and phytoliths (KOU-AR6-06 PN-10 to PN-15). At top right, macrofossil and microfossil sampling for oyster-rich deposits extracted through the excavator bucket, lower in the marine sequence (not visible). Photograph by L.M.

Nature: trench
Investigated in: October 7, 2021
Access: excavated and filled up immediately
Amount of sediment sampled: 255 kg in basal conglomerates and grey-kaki clays (Base); 15 kg in kaki clays (Top)
Handpicking: yes
Screenwashing: yes
Sampled for: Macrofossils, Microfossils, Pollen, U-Th dating, OSL dating, ^{14}C dating

2. Methods

2.1. Fossil preparation, extraction, and analysis

2.1.1. Macrofossil and microfossil sampling, screen-washing, and subsequent study

All the fossil remains described here were found in-situ by our consortium in 2018, 2019, and 2021. Some macro-remains (e.g., oysters, wood chunks, and large selachian teeth) were hand-picked directly in the field and properly located/labelled. All other fossil specimens were collected by screening-washing of clays, silts, and conglomerates, with a 2 mm, 1 mm, and/or 0.7 mm mesh. Smaller sieves were used for microvertebrates (0.4 mm) and foraminifers (150 and 63 µm). Foraminifers were only retrieved within connected valves of large bivalves. Their absence in all other marine samples is most likely due to post-burial dissolution of their tests, which likely further resulted in a lower taxonomic diversity recorded. No acid etching has been performed, in order to preserve delicate calcified shells, either visible or invisible to the unaided eye.
The fossil specimens were curated in separate ziplocks with adequate labels (location/date/sampling locality/sampling level/subsample, etc.), and subsequently sent to colleagues with the best expertise on the taxonomic group concerned. Over 1,000 kg of sediment have been screen-washed in total.

2.1.2. Charcoal identification

Charcoals were manually broken according to the three planes of wood – transverse, radial longitudinal and tangential longitudinal – and observed under a reflected light microscope equipped with dark and bright fields at x10, x20 and x50 magnifications. Charcoal identification was performed after comparison with the wood charcoals from the reference collection from French Guiana located at the Institut des Sciences de l'Evolution de Montpellier (1) and with the help of identification tools (2–4).

2.1.3. Phytolith extraction and analysis

After adding 56.000 microspheres, the phytolith samples were boiled four times in 33% H_2O_2 and treated with 10% HCl and $KMnO_4$ to remove organic matter. After decanting, phytoliths were extracted using Bromoform (specific gravity 2.3) (5) and mounted on microscope slides using Permount. Phytoliths were counted using the Zeiss Axioscope. For samples PN15A and PN15B, a sum of 400 phytoliths were counted at 630X magnification. For samples PN9-PN14, the concentration of phytoliths was too low to obtain a full count. Instead, the slides were scanned at 400X magnification. Phytolith morphotypes were classified according to literature (6–8).

2.1.4. Pollen extraction and analysis

**KOU-AR6-03 trench*

Nine samples of 1 and 2 cm^3 from nine different depth intervals (PN0–PN8, see Fig. S11) were processed for pollen analysis. Only PN6 yielded a decent pollen recovery, with not enough grains for being counted, though.

**KOU-AR6-06 trench*

Eleven subsamples of 1 and 2 cm^3 from seven different depth intervals (PN9–PN15, see Fig. S11) were processed for pollen and phytolith analysis. Pollen samples were processed conform standard palynological extraction procedures (9). *Lycopodium* tablets were added to allow the calculation of pollen concentration. A minimum of 300 pollen grains was counted using a 400x magnification light microscope. Fern spores other than *Acrostichum*, and Cyperaceae were not included in the pollen sum. Results are presented as a percentage of the pollen sum. Samples PN10 – PN14 were completely devoid of pollen. Therefore, only samples from two depth intervals (PN9 and PN15) could be counted.

2.2. Dating methods

2.4.1. Optically-Stimulated Luminescence (OSL)

Samples for OSL dating were collected with metal tubes pounded into fresh sediment, and have been prepared at the Institute of Geological Sciences (Univ, Bern) following the protocol described in Lowick et al. (10). Under subdued laboratory illumination, samples were treated with HCl (32%) and H_2O_2 (30%) to remove carbonates and organic components, respectively. Quartz fine-sand fractions were isolated following sieving (63-100µm) and density separation using LST Fastfloat heavy liquid at 2.70 g cm^{-3}. The fine-grained quartz was etched in 40% hydrofluoric acid for 1 h (to remove any feldspar contamination), rinsed and then immersed in 32% hydrochloric acid for 1 h to remove fluorides. Fine quartz grains were settled on 10-mm diameter stainless steel discs using silicon spray (4-mm diameter mask).

All luminescence measurements were carried out using TL/OSLDA-20 Risø readers, equipped with a calibrated $^{90}Sr/^{90}Y$ beta source (Institute of Geological Sciences, Univ. Bern). Luminescence signals were detected using an EMI 9235QA photomultiplier tube, with stimulation at 90% power using blue LEDs at 125°C, and with the signal detected through 7.5-mm of Hoya U-340 transmission filter.

All equivalent dose (De) measurements were performed using a modified (post-IRSL) SAR protocol (11, 12). A preheat of 200°C for 10 s was applied to ensure that the protocol was able to recover a regenerated dose to within 10% of unity (and in addition this protocol provided low/negligible residuals). De values were calculated using the first 0.8 s of the OSL signal, using an early background correction (first 10s after OSL signal integral) and an exponential fitting for constructing the dose-response curves. All aliquots met the following criteria: (1) recycling ratios within 10% of unity, (2) recuperation values below 10%, and (3) IR-depletion ratio below 15% (13).

About 100 g of bulk sediment material was collected from the surrounding of each sample to determine the environmental dose rate. The material was desiccated at 60 °C to enable water content quantification. U, Th and K activities were measured using high-resolution gamma spectrometry [Department of Chemistry and Biochemistry, Univ. Bern (14)] and were employed, together with the measured water content, as inputs for final dose rate determination through the Dose Rate and Age Calculator [DRAC (15)]. We used the Luminescence R package (16) to quantify the Central Age Model (CAM) (17) for both samples.

2.4.2. U-Th dating (conventional solution)

Conventional solution U/Th dating of coral fragments from KOU-AR6-06 (base) has been carried out using a Thermo Neptune plus at GEOMAR Helmholtz Center for Ocean Research Kiel, Germany. The procedures (chemical preparation and separation, analyses) followed the approach described by Fietzke et al. (18). This included the use of a Th229/U233/U236 mix spike, added after sample dissolution prior to the chemical separation of the Th and U from the sample matrix. The results of this analysis are summarized in Table S4.

For the correction of non-radiogenic Th230 a detrital Th230/Th232 activity ratio of 0.6 ± 0.2 has been applied. The back-calculated initial U234/U238 activity ratio is slightly higher than the typical open-ocean ratio, which is taken as indication of a small potential loss of uranium from the sample. Considering this, the calculated age should be interpreted as a maximum value.

2.4.3. U-Th dating (laser ablation)

Twelve *Astrangia rathbuni* corals were sampled at the bottom of the KOU-AR6-03 trench, to obtain uranium-series ages. Uranium-series measurements were undertaken by laser ablation Multi Collector-Inductively Coupled Plasma Mass Spectrometer (MC-ICPMS) at the Geoarchaeology and Archaeometry Research Group (GARG) Biomics facility, Southern Cross University. Laser ablation was performed with a New Wave Research 213 nm laser, equipped with a TV2 cell. Thorium (^{230}Th, ^{232}Th) and uranium (^{234}U, ^{235}U, ^{238}U) isotopes were measured on a Thermo Neptune XT MC-ICPMS mounted with jet sample and x-skimmer cones. All five isotopes were collected in static mode, with both ^{234}U and ^{230}Th collected in the ion counter and CDD respectively. Helium flow rate and ICP-MS parameters were tuned with NIST610 element standard to derive a ^{232}Th/^{238}U ratio greater than 0.80. Tuning was achieved with a fluence of 10.3 J/cm2, pulse rate of 20 Hz, spot size of 110 µm and scan speed of 5 µm/s, yielding 1.91V of ^{238}U and 1.57V of ^{232}Th on NIST610.

Because of their size, samples had to be mounted in resin and then polished to 5micron smoothness. Each sample was then ablated using rasters of 5min each (twice ~750 µm long). Before and after each sample, NIST612, MK10 and MK16 (19) standards were measured. ^{234}U/^{238}U and ^{230}Th/^{238}U isotopic ratios were corrected for elemental fractionation and Faraday cup/SEM yield by comparison with MK10 coral for which ratios were previously characterized internally by solution analysis. Detrital-corrected ^{230}Th-U ages were calculated for each analysis using IsoPlotR (20) with an assumed detrital (^{230}Th/^{232}Th) activity ratio of 0.8 ± 0.8. Concentrations of U and Th were determined using NIST612 glass as a calibration standard. Background subtraction, concentration quantification and ratio corrections were performed using Iolite™ software (21). The corrected (^{234}U/^{238}U) and (^{230}Th/^{238}U) isotope ratios for the secondary standard (MK16 coral) within error of the value determined by solution analysis.

2.4.4. Radiocarbon analysis

Charcoals were identified before being sent for dating to ensure they belong to different taxa and hence from different individuals (22). Furthermore, whenever possible, charcoals from twigs or short-lived taxa were selected for dating to avoid the old wood effect (23).

Charcoal samples were dated at the Accelerator Mass Spectrometry Laboratory, Center for Physical Sciences and Technology in Vilnius (Vilnius Radiocarbon). Before radiocarbon (^{14}C) measurements, the samples had to be graphitized first. Graphitization was performed with Automated Graphitization System (AGE-3, Ionplus AG). Chemical preparation of charcoal samples was performed using the standard acid–base-acid method (24). The chemical treatment steps were as follows: 1M hydrochloric acid, 0,1M sodium hydroxide and 1M hydrochloric acid. A Single-stage Accelerator Mass Spectrometer (SSAMS, NEC, USA) was used for radiocarbon measurements. Phthalic anhydride was used for the estimation of the background of measurements (2.45 × 10−3 fM (fraction of modern carbon)). The NIST-OXII (134.06 pMC) standard was used as reference material. The ^{14}C/^{12}C ratio was measured with an accuracy better than 0.3%. For the isotopic fractionation correction, the ratio of ^{13}C to ^{12}C was used. All dates were calibrated by OxCal v4.4.4 (25) following the IntCal20 atmospheric curve (26).

3. Results

3.1. Age constraints

3.1.1. OSL age constraints

For OSL dating, luminescence measurements showed that almost all aliquots were close to saturation, and thus to the dating limit of the quartz OSL method. As a consequence, OSL age constraints must be taken as minimum age estimates, given that the coastal depositional environments for these sediments would a priori present any major issue of pre-depositional partial bleaching of the OSL signal. For

discussion, we estimated two OSL age constraints for samples OSL-1 and OSL-2, either considering all aliquots providing a De value (column 5 in Table S2) or by considering only aliquots below saturation (column 6 in Table S3). OSL results show very similar age estimates (within errors) for the two samples, and in the main text we report minimum age estimates using only aliquots below saturation.

***Table S2*.** OSL dating results. Analytical details and measurement protocols are given in the main text.
[1]A total of 24 aliquots have been measured for each sample. Some aliquots did not provide any D_e value (natural OSL signal on/above the dose-response plateau), and for aliquots with D_e values some were in saturation [D_e>2*D_0 (27)].
[2-3]De = Equivalent doses (non-corrected for residuals), CAM = Central Age Model, OD = overdispersion of D_e distribution (17). For (2), CAM D_e values and OSL ages have been estimated using all aliquots providing a D_e estimate. For (3), CAM D_e values and OSL ages have been estimated using all non-saturated aliquots.

Sample	Nb aliquots[1] (D_e/Non-saturated)	CAM[2] D_e (Gy) *(OD %)*	CAM[3] D_e (Gy) *(OD %)*	CAM OSL[2] age (ka)	CAM OSL[3] age (ka)
OSL-1	6/1	225.1±14.1 (*8.9*)	194.9±10.5 (*/*)	138.3±12.6	119.7±10.2
OSL-2	8/2	233.2±24.1 (*26.4*)	168.9±26.5 (*21.1*)	144.4±17.9	104.6±17.9

***Table S3*.** Details of dose-rate calculations for OSL dating.
[1]Radionuclide concentrations were quantified on bulk samples using high-resolution gamma spectrometry (Department of Chemistry and Biochemistry, Univ. Bern).
[2]Dose rate calculations were performed with DRAC (15), assuming water content of 25±10% and bulk sample density of 2.3±0.3 g cm^{-3}.

Sample	Radionuclide concentration[1]			Grainsize (µm)	Depth below surface (m)	Total dose rate[2] (Gy ka^{-1})
	U (ppm)	Th (ppm)	K (%)			
OSL-1	2.03±0.11	5.93±0.30	0.99±0.05	63-100	2.1±0.1	1.628±0.11
OSL-2	1.79±0.18	6.13±0.31	1.04±0.05	63-100	3.0±0.1	1.615±0.11

3.1.2. U-Th ages

***Table S4*.** Results of conventional solution MC-ICP-MS U-Th dating of the coral *Astrangia rathbuni*, from KOU-AR6-06 (base).

Sample	Age	±	min-Age	max-Age	U238	±	Th232	±
	ky	ky	ky	ky	ppm	ppm	ppb	ppb
#12 Kourou	**135,8**	**1,1**	**134,7**	**136,9**	2,7922	0,0023	343	3

Sample	Th230	±	Th230/Th232	±	U238/Th232	±	Th230/U238	±
	ppt	ppt	dpm/dpm	dpm/dpm	dpm/dpm	dpm/dpm	dpm/dpm	dpm/dpm
#12 Kourou	38,210	0,049	20,83	0,16	25,23	0,20	0,82541	0,00126

Sample	Th230excess/U238	±	U234/U238	±	U234/U238initial	±	238/232	232/238
	dpm/dpm	dpm/dpm	dpm/dpm	dpm/dpm				
#12 Kourou	0,80164	0,00188	1,108	0,00166	1,158	0,002	25,23	0,039628868

Table S5. Details of U-Th dating results on corallites of *Astrangia rathbuni* from KOU-AR6-03 (base). Ages and standard errors taken into account in the current work are bold-typed and in blue (Coral-2 and Coral_6 to Coral_12).

	U_ppm	U_ppm_Int2SE	R48	Err_R48_Int2SE	R08	Err_R08_Int2SE	Age (ka)	Err (2-SE)
Coral_1	1.04	0.38	1.13	*0.21*	*0.65*	*0.59*		
Coral_2	0.98	0.13	1.123	0.049	0.802	0.098	**127.6998**	**25.5399**
Coral_3	2.55	0.57	1.101	0.044	*0.928*	*0.93*		
Coral_4	2.62	0.71	1.059	0.038	*1.049*	*0.68*		
Coral_5	4.7	1.9	1.083	0.038	*1.054*	*0.087*	***262.4702***	***80.9658***
Coral_6	3.33	0.12	1.122	0.024	*1.04*	*0.054*	***220.5032***	***32.4994***
Coral_7	3.38	0.25	1.137	0.021	0.915	0.054	**124.9245**	**14.3312**
Coral_8	3.93	0.17	1.133	0.019	0.95	0.087	**142.6015**	**28.5683**
Coral_9	3.73	0.21	1.131	0.035	0.894	0.035	**145.0988**	**9.3231**
Coral_10	4.72	0.19	1.134	0.025	0.798	0.034	**127.1405**	**6.9228**
Coral_11	4.9	0.46	1.128	0.018	0.8	0.042	**129.1681**	**11.4697**
Coral_12	3.655	0.072	1.164	0.028	0.802	0.047	**122.0262**	**10.3722**

3.1.3. Radiocarbon datings

Table S6. Charcoal sample designation (field number / lab code) and radiocarbon ages obtained (BP and *cal* BP, using OxCal;

Sample designation	Lab. code	Radiocarbon age, BP	Radiocarbon age, *cal* BP
KOU-AR6-04-SITU-3-RUB	FTMC-HE52-3	892±30	804±55
KOU-AR6-04-SOM-40-SM	FTMC-HE52-1	1995±88	1938±120
KOU-AR6-04-LIT-2-INDET	FTMC-HE52-2	39825±288	43091±284
KOU-AR6-04-?-22-MLT	FTMC-HE52-4	44717±478	47053±572

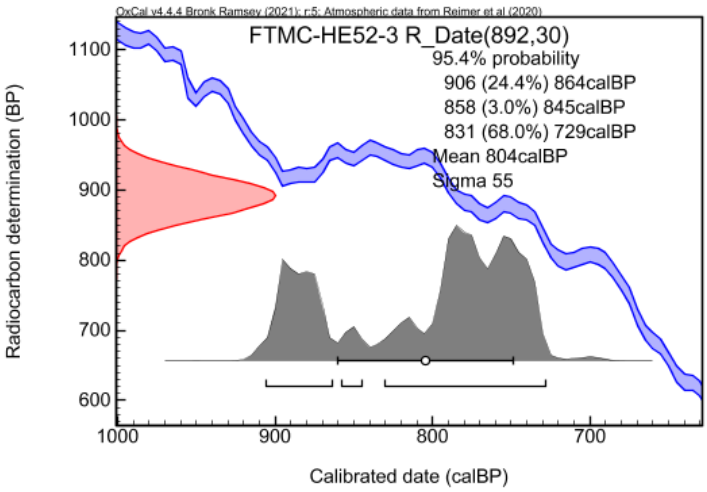

Fig. S7. Calibrated radiocarbon date before present obtained for the uppermost charcoal sample (KOU-AR6-04-SITU-3-RUB), Unit C, Top at KOU-AR6-04, through OxCal v 4.4.4 [online version (25)].

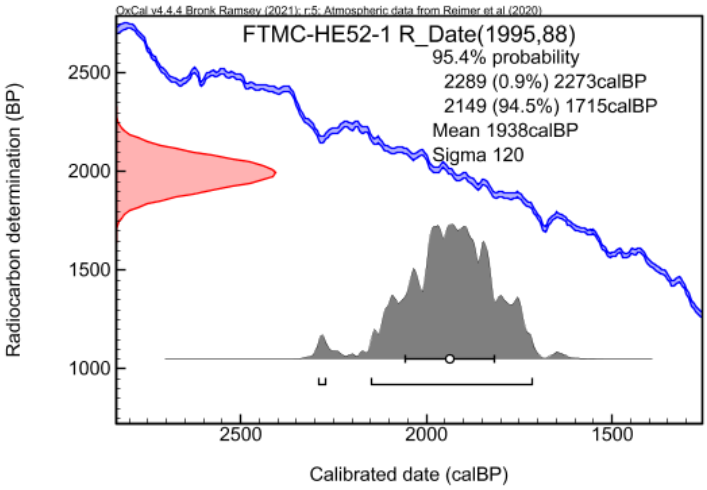

Fig. S8. Calibrated radiocarbon date before present obtained for the second uppermost charcoal sample (KOU-AR6-04-SOM-40-SM), Unit C, Top at KOU-AR6-04, through OxCal v 4.4.4 [online version (25)].

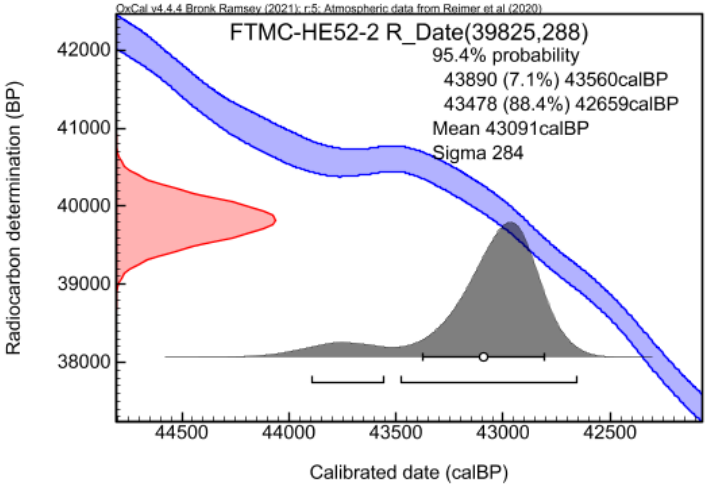

Fig. S9. Calibrated radiocarbon date before present obtained for the second lowermost charcoal sample (KOU-AR6-04-LIT-2-INDET), Unit C, Base at KOU-AR6-04, through OxCal v 4.4.4 [online version (25)].

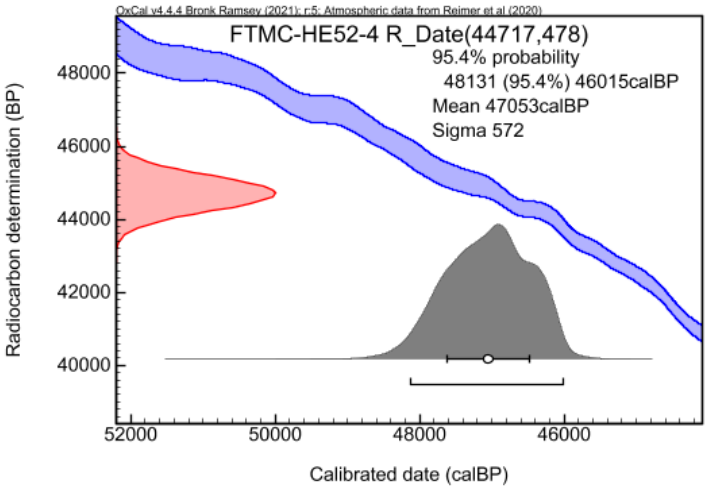

Fig. S10. Calibrated radiocarbon date before present obtained for the lowermost charcoal sample (KOU-AR6-04-?-22-MLT), Unit C, Base at KOU-AR6-04, through OxCal v 4.4.4 [online version (25)].

3.2. Stratigraphic sections

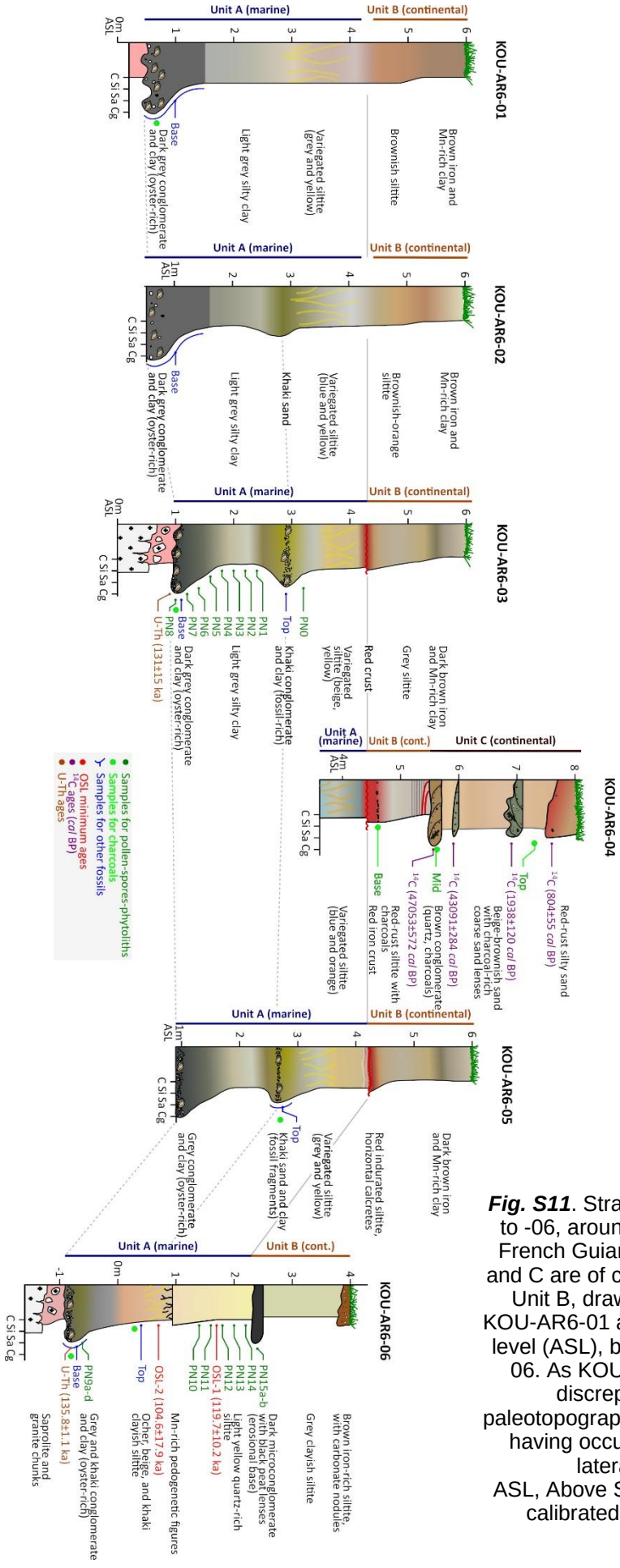

Fig. S11. Stratigraphic sections of trenches KOU-AR6-01 to -06, around the Kourou ELA4 launcher pad, Kourou, French Guiana. Unit A is of marine origin, while Units B and C are of continental origin (cont.). The baseline of the Unit B, drawn in grey, is horizontal between sections KOU-AR6-01 and -05, at 4.2–4.5 m above the recent seal-level (ASL), but it is dropping to 2.4 m ASL at KOU-AR6-06. As KOU-AR6-06 was located more seaward, this discrepancy is interpreted as resulting from paleotopography instead of differential vertical movements having occurred in the meantime. Doted lines denote laterally-equivalent levels in the Unit A.
ASL, Above Sea-Level; BP, Before Present; C, clay; *cal*, calibrated; Cg, conglomerate; Sa, sand; Si, siltite.

3.3. Taxonomic composition of Kourou ELA 4 biotic communities

3.3.1. Foraminifers

Communities formed by foraminifers (Fig. 2A–C) are mainly composed of hyaline-perforate benthic taxa, indicative for shallow intertidal mangrove and subtidal environments (11 species and seven genera) and one individual of planktonic foraminifer (*Globigerina bulloides;* Fig. 2D) (*SI Appendix*, Table S7). Their fine preservation state suggests low energy and preservation in-situ. The benthic assemblage comprises three species of Miliolida (*Quinqueloculina seminula*, *Q*. sp. 1 and *Q*. sp. 2) and eight species of Rotaliida, including three species of *Ammonia*, *Eponides repandus*, and very small foraminifer species (*Nonion subturgidum*, *Elphidium magellanicum*, *Cerebrina claricerviculata*, and *Fursenkoina* sp.). These very small species usually live in low-oxygenated sediments, while *Ammonia* tolerate low-salinity conditions and potentially occur in mangrove habitats and estuaries with variable salinity conditions. All other benthic foraminifers are comparatively shallow marine, subtidal taxa, usually occurring in nearshore shallow-water environments characterized by algae or seagrass vegetation. The area was not hosting a typical reef or lagoon environment (absence of large symbiont-bearing foraminifers) and the open ocean influence was low. All 12 foraminifer species occur at the top of the KOU-AR6-05 section. With 90 individuals (71 in KOU-AR6-03), *Eponides repandus* is the most dominant foraminifer species in all trenches, like in the foraminifer associations observed in a mangrove estuary from northern Brazil, with a substantial marine influence through tides (28).

***Table S7*.** Composition of KOU-AR6 foraminifer assemblages and individual abundances, earliest Late Pleistocene, Kourou, French Guiana.

Sample Number	*Quinqueloculina seminula*	*Quinqueloculina* sp. 1	*Quinqueloculina* sp. 2	*Ammonia veneta*	*Ammonia tepida*	*Ammonia parkinsoniana*	*Elphidium magellanicum*	*Nonion subturgidum*	*Eponides repandus*	*Furskenkoina* sp.	*Cerebrina claricerviculata*	*Globigerina bulloides*
KOU-AR6-01 (Base)									3			
KOU-AR6-03 (Base)	2	1		14	11	1			71			
KOU-AR6-05 (Top)	5	3	2	3	1	1	2	5	8	1	1	1
KOU-AR6-06 (Base)								1	8			
Total number	7	4	2	17	12	2	2	6	90	1	1	1

3.3.2. Metazoans

Cnidarians

Cnidarians are documented by an octocorallian gorgonian (one specimen of *Pacifigorgia*, at KOU-AR6-06; Fig. 2G) and >1700 specimens of a single scleractinian species, *Astrangia rathbuni*, either growing as solitary corallites or small colonies (Fig. 2F). *Astrangia rathbuni* was recognized in all sampled marine levels, with a much higher density at KOU-AR6-06 than in other trenches. Solitary corallites dominate over colonies at KOU-AR6-06 and -05 Top, notably with respect to -03 (Base and Top) (*SI Appendix*, Table S8).

***Table S8*.** Composition of KOU-AR6 *Astrangia rathbuni* assemblages, earliest Late Pleistocene, Kourou, French Guiana.

Locality	Layer	Sampled sediment (W) [kg]	Solitary	Colonial	Total (N)	Density (N/W)	Ratio (Solitary/ total)
KOU-AR6-01	basal	>100	90	93	183	<1.83	0.49
KOU-AR6-03	basal	320	113	182	295	0.92	0.38
KOU-AR6-03	top	30	12	19	31	1.03	0.39
KOU-AR6-05	top	150	43	21	64	0.43	0.67
KOU-AR6-06	basal	255	804	353	1157	4.53	0.69
Total		>855	1062	668	1730	<2.02	0.61

Bryozoans

The trenches KOU-AR6-01, -03 and -05 yielded an unexpected taxonomic diversity of **bryozoans** mostly typical of tropical shallow waters, with 379 specimens assigned to 19 species, 12 genera and 11 families. Four species (*Biflustra arborescens*, *B*. cf. *savartii*, *Conopeum* sp. and *Steginoporella magnilabris*; Fig. 2H–J) occur in all sampled levels. More generally, bryozoans are much more abundant and diverse in the basal oyster-rich grey clays than in the khaki conglomerates (*SI Appendix*, Table S9). Most of these taxa also occur in the present-day coastal waters of Brazil [e.g., (29, 30)]. Warm-water genera (*Biflustra*, *Steginoporella*, *Antropora* and *Nellia*) are well represented in both recent and fossil Kourou records. The predominance of encrusting ‘anascans’ suggests a shallow depositional environment affected by freshwater influxes associated with increased turbidity, as in mangrove and oyster-rich settings (31). Among lophotrochozoans, around 200 calcareous tubes of unidentified polychaete worms are documented in the marine sequence of all trenches (half of the specimens do originate from (KOU-AR6-01).

***Table S9*.** Composition of KOU-AR6 bryozoan assemblages, earliest Late Pleistocene, Kourou, French Guiana.

KOU-AR6-01 (basal oyster-rich grey clays)		KOU-AR6-03 (basal oyster-rich grey clays)		KOU-AR6-03 (kaki conglomerate)		KOU-AR6-05 (kaki conglomerate)		KOU-AR6-06 (basal oyster-rich kaki clays)		
Antropora sp.	1							Anasca indet. (small fragments)	3	
Biflustra arborescens	119	*Biflustra arborescens*	63	*Biflustra arborescens*	22	*Biflustra arborescens*	8			
Biflustra cf. *grandicella*	1									
				Biflustra irregulata	1					
Biflustra marcusi	1									
Biflustra cf. *savartii*	3	*Biflustra* cf. *savartii*	16	*Biflustra* cf. *savartii*	4	*Biflustra* cf. *savartii*	3			
Biflustra tenuis	3									
						Conopeum loki	1			
Conopeum sp.	20	*Conopeum* sp.	12	*Conopeum* sp.	2	*Conopeum* sp.	1			
		Crisia sp.	33							
Ellisina sp.	3									
Membranipora sp.	3			*Membranipora* sp.	1					
		Nellia tenella	17							
						Parasmittina sp.	1			
		Quadricellaria sp.	1							
		Savignyella lafontii	3							
		Smittoidea, fam. gen. et sp.	1							
Steginoporella magnilabris	14	*Steginoporella magnilabris*	10	*Steginoporella magnilabris*	2	*Steginoporella magnilabris*	3			
		Watersipora sp.	3							**specimens**
10 species	168	**10 species**	159	**6 species**	32	**6 species**	17	**1 species**	3	379

Mollusks

Mollusks vastly dominate other phyla in both taxonomic diversity and specimen numbers (Fig. 2L–Y). They include two species of scaphopods (*Antalis antillarum* and *Dentalis laqueatum*; only a few shells), 35 species of bivalves and 50 species of gastropods. Bivalves and snails are recorded by thousands of individuals in all marine levels that were sampled, with shallow water *Costoanachis avara* (Fig. 2S), *Sheldonella bisulcata* (Fig. 2N), and *Chione cancellata* (Fig. 2W) most abundant. In terms of richness and evenness, KOU-AR6-03 is most diverse with 59 species (for 685 specimens), whereas KOU-AR6-06 yields only 30 species (for 1666 specimens; *SI Appendix*, Table S10). The state of preservation is exquisite for several specimens which retain colored patterns visible to the naked eye [e.g., *Vitta* (Fig. 2Q), *Pilsbryspira*] or revealed under UV light [e.g., *Crassinella*, *Olivella*; Fig. 2Y]. Most molluscan taxa have affinities to intertidal and shallow subtidal sands, muds, or rocks and several species are characteristic of mangrove habitats (e.g., *Vitta virginea*, *Isognomon radiatus*).

***Table S10*.** Composition and abundance of KOU-AR6 molluscan assemblages, earliest Late Pleistocene, Kourou, French Guiana.

Class	Family	Species	KOU-AR6-01	KOU-AR6-03	KOU-AR6-05	KOU-AR6-06
Gastropoda	Amathinidae	*Iselica globosa*		1	15	110
Gastropoda	Ampullariidae	*Asolene* sp.	1			
Gastropoda	Ampullariidae	*Pomacea* sp.	1			
Gastropoda	Architectonicidae	*Heliacus bisulcatus*	40	5	28	68
Gastropoda	Buccinidae	*Engina turbinella*		X		
Gastropoda	Caecidae	*Caecum rhyssotitum*			5	
Gastropoda	Cerithiidae	*Bittiolum varium*				50
Gastropoda	Cerithiopsidae	*Cerithiopsis gemmulosum*		1	1	
Gastropoda	Cerithiopsidae	*Cerithiopsis* sp.		2		
Gastropoda	Cerithiopsidae	*Seila adamsii*			3	10
Gastropoda	Columbellidae	*Astyris lunata*		5	16	10
Gastropoda	Columbellidae	*Cosmioconcha* sp.	1			
Gastropoda	Columbellidae	*Costoanachis avara*	1	20	1	
Gastropoda	Columbellidae	*Parvanachis obesa*	1	120	108	200
Gastropoda	Cylichnidae	*Cylichna discus*		X		
Gastropoda	Epitoniidae	*Depressicala nitidella*	5	1		10
Gastropoda	Epitoniidae	*Gyroscala lamellosa*	80	4		150
Gastropoda	Eratoidae	*Archierato maugeriae*	1		1	
Gastropoda	Eulimidae	*Eulima bifasciata*	6	4	1	
Gastropoda	Fissurellidae	*Diodora cayenensis*	18	22		50
Gastropoda	Fissurellidae	*Lucapina sowerbii*	4			5
Gastropoda	Haminoeidae	*Cylichnella bidentata*		5	26	150
Gastropoda	Melongenidae	*Melongena melongena*		1		
Gastropoda	Muricidae	*Stramonita haemastoma*	1	4	6	8
Gastropoda	Nassariidae	*Phrontis vibex*		1		
Gastropoda	Naticidae	*Naticarius marochiensis*			1	X
Gastropoda	Naticidae	*Naticarius canrena*				X

Gastropoda	Naticidae	*Stigmaulax cayennensis*		6	1	X
Gastropoda	Naticidae	*Naticidae indet.*				14
Gastropoda	Neritidae	*Vitta virginea*	6	7	3	
Gastropoda	Olivellidae	*Olivella lactea*		25		
Gastropoda	Olivellidae	*Olivella minuta*	100	20		
Gastropoda	Olivellidae	*Olivella myrmecoon*		2		
Gastropoda	Ovulidae	*Pseudocyphoma intermedium*		2		
Gastropoda	Ovulidae	*Simnialena uniplicata*		2		
Gastropoda	Pyramidellidae	*Bonnea jadisi*				50
Gastropoda	Pyramidellidae	*Chrysallida gemmulosa*		X		
Gastropoda	Pyramidellidae	*Pyrgolampros* sp.		1		100
Gastropoda	Pyramidellidae	*Turbonilla pusilla*			1	
Gastropoda	Pyramidellidae	*Turbonilla* sp.				60
Gastropoda	Pyramidellidae	*Turbonilla rixtae*		2		
Gastropoda	Pseudomelatomidae	*Pilsbryspira leucocyma*		3		
Gastropoda	Terebridae	*Impages cinerea*		1		7
Gastropoda	Terebridae	*Neoterebra dislocata*			8	
Gastropoda	Tornidae	*Cyclostremiscus* sp.			1	
Gastropoda	Triphoridae	*Monophorus olivaceus*			10	
Gastropoda	Triphoridae	*Triphora intermedia*		2		22
Gastropoda	Mangeliidae	*Kurtziella serga*		2		29
Gastropoda	Turridae	Turridae indet.				15
Gastropoda	Vermetidae	*Petaloconchus mcgintyi*			1	
Bivalvia	Anomiidae	*Pododesmus rudis*		1		
Bivalvia	Arcidae	*Acar domingensis*	2	8		3
Bivalvia	Arcidae	*Arca imbricata*	1			
Bivalvia	Arcidae	*Anadara chemnitzii*	1	1		
Bivalvia	Arcidae	*Cucullaearca candida*	1	1		2
Bivalvia	Arcidae	*Lunarca ovalis*	9	19	1	
Bivalvia	Cardiidae	*Dallocardia muricatum*	1	1		
Bivalvia	Chamidae	*Chama radians*	2	2		
Bivalvia	Corbulidae	*Caryocorbula contracta*	40	103	6	45
Bivalvia	Corbulidae	*Hexacorbula dietzana*		4		5
Bivalvia	Crassatellidae	*Crassinella lunulata*	33	2	1	75
Bivalvia	Dimyidae	*Dimya acuminata*		X		
Bivalvia	Isognomonidae	*Isognomon radiatus*		X		
Bivalvia	Leptonidae	*Lepton lepidum*		X		
Bivalvia	Mactridae	*Mulinia cleryana*	60	51	7	
Bivalvia	Mytilidae	*Gregariella chenui*		2		
Bivalvia	Mytilidae	*Brachidontes domingensis*		1		
Bivalvia	Noetiidae	*Arcopsis adamsi*		3	4	
Bivalvia	Noetiidae	*Sheldonella bisculcata*	23	83	10	120
Bivalvia	Nuculanidae	*Nuculana concentrica*	1	4		
Bivalvia	Nuculidae	*Ennucula puelcha*		1		
Bivalvia	Ostreidae	*Crassostrea rhizophorae*		10		3
Bivalvia	Pectinidae	*Argopecten gibbus*			1	
Bivalvia	Pectinidae	*Leptopecten bavayi*	56	23	4	95
Bivalvia	Plicatulidae	*Plicatula gibbosa*	2	46	1	50
Bivalvia	Pteriidae	*Pteria colymbus*		1		
Bivalvia	Semelidae	*Cumingia lamellosa*		1		
Bivalvia	Telinidae	*Angulus diantha*		2		
Bivalvia	Telinidae	*Eurytellina* sp.		1		
Bivalvia	Telinidae	*Strigilla* sp.		1		
Bivalvia	Telinidae	*Tampaella mera*		1		
Bivalvia	Thraciidae	*Asthenothaeus* sp.		1		
Bivalvia	Ungulinidae	*Diplodonta soror*		1		
Bivalvia	Veneridae	*Chione cancellata*	122	37	13	150
Bivalvia	Yoldiidae	*Orthoyoldia crosbyana*	1			
Scaphopoda	Dentaliidae	*Antalis antillarum*		1		
Scaphopoda	Dentaliidae	*Dentalium laqueatum*		1		

Arthropods

The crustacean arthropods are particularly dominant at Kourou, with thousands of specimens retrieved from the sediments, all belonging to either barnacles (balanomorph cirripeds), crabs or shrimps (decapods). The barnacles are represented by *Amphibalanus* sp. and an unidentified small balanid, with a large amount of disconnected wall plates found in all sampled localities, and a single complete

specimen (at KOU-AR6-01; Fig. 2Z). The decapods are represented mostly by hundreds of isolated claw remains, mainly of mobile and fixed fingers, with only a few other claw and carapace remains recovered. Decapod remains are much less abundant and poorly preserved in KOU-AR6-06 with respect to other trenches (*SI Appendix*, Table S11). The decapods comprise eight morphotypes, including two species of mud shrimps, three species of hermit crabs, and three species belonging to the true crabs. The mud shrimps, include ghost shrimps (*Neocallichirus* sp. (Fig. 2A'–B')) and Callichiridae indet. (Fig. 2C'–D'). Hermit crabs include porcelain crabs such as *Pachycheles* sp. (Fig. 2E') and *Petrolisthes* sp. (Fig. 2F'), which are filter feeders found in reefs, under rocks, shell beds, or mangroves. Small claw fragments further document a possible paguroid. The true crabs are represented by stone crabs (*Eriphia*/*Menippe*; Fig. 2G'–H'), crabs feeding on hard-shelled mollusks, including oysters. In addition, remains of the purse crab (?*Persephona* sp. (Fig. 2I')), and a swimming crab (Portunidae indet., Fig 2J') were found, but also small claw fragments of a spider crab (?Majoidea indet.) and a box crab (?*Hepatus* sp.). The overall decapod association indicates proximity to mangroves, with soft sediments hosting *Neocallichirus* mud shrimps (feeding on seagrass and algae) and purse crabs *Persephona*. This association points to intertidal–subtidal tropical to temperate waters (0–50 m), with Western Atlantic, Caribbean, and tropical Eastern Pacific affinities (*Persephona*).

***Table S11*.** Composition of KOU-AR6 decapod crustacean assemblages, earliest Late Pleistocene, Kourou, French Guiana.

Clade/Superfamily/Family	Taxon	KOU-AR6	KOU-AR6-01	KOU-AR6-03	KOU-AR6-05	KOU-AR6-06	Total	Approx. ranges
Axiidea: Callichiridae	*Neocallichirus* sp.	125	637	700	8	18	**1488**	>1000
Axiidea: Callichiridae	Callichiridae indet.	28	23	10			**61**	10–100
Anomura: Galatheoidea: Porcellanidae	*Pachycheles* sp.		5	1			**6**	1–10
Anomura: Galatheoidea: Porcellanidae	*Petrolisthes* sp.		77				**77**	10–100
Anomura: Galatheoidea: Porcellanidae	Porcellanidae indet.	66	75	16			**157**	100–200
Anomura: Paguroidea	?Paguroidea indet.			1			**1**	1
Brachyura: Majoidea	? Majoidea indet.			1			**1**	1
Brachyura: Leucosioidea: Leucosiidae	? *Persephona* sp.		1	1			**2**	1–5
Brachyura: Aethroidea: Aethridae	? *Hepatus* sp.		1				**1**	1
Brachyura: Portunoidea: Portunidae	Portunidae indet.	8	23	16		5	**52**	10–100
Brachyura: Eriphioidea	*Eriphia* /*Menippe*	60	35	64	11	73	**243**	100–500

Echinoderms

Echinoderms were retrieved in high numbers in all marine samples, nevertheless pointing to a low taxonomic diversity (three species). The echinoderm community is overdominated by the Atlantic purple sea urchin (*Arbacia punctulata*; Fig. 2K), easily recognizable through 1985 spines, but also by 138 jaw and test fragments from all sampled levels and trenches (*SI Appendix*, Table S12). In stark contrast, other echinoderm specimens include only a few dozens of test fragments of two unidentified heart urchins (one and 67 specimens) and two plates of an astropectinid sea star, sampled in the basal grey level at KOU-AR6-01 and in the khaki conglomerate at KOU-AR6-03 (Top).

***Table S12*.** Composition of KOU-AR6 echinoderm assemblages, earliest Late Pleistocene, Kourou, French Guiana.

Taxon	***comments***	***KOU-AR6-01 grey clays***	***KOU-AR6-03 grey oyster-rich clays***	***KOU-AR6-03 kaki conglomerate***	***KOU-AR6-05 kaki conglomerate (top)***	***KOU-AR6-06 basal clays***	***Total specimens per taxon***
Arbacia punctulata	Fragments of sea urchin jaw **(hemipyramid)**		**12**	**13**		**1**	
	Fragments of sea urchin jaw **(rotula)**			**3**			
	Fragments of sea urchin jaw **(epiphysis)**			**1**		**1**	***2123***
	Complete **primary spines**	**76**	**251**	**325**	**49**	**225**	
	Fragments of **primary spines**	**256**	**20**	**82**	**41**	**660**	
	Test fragments (Ambulacral and interambulacral plates)	**34**		**54**	**2**	**17**	
Spatangoida indet. 1	**Test fragments** (Ambulacral and interambulacral plates)			**1**			**1**
Spatangoida indet. 2	**Test fragments** (Ambulacral and interambulacral plates)	**52**		**15**			**67**
Astropectinidae indet.	**Inferomarginal plate**	**1**		**1**			**2**
	Total specimens per sampling locality	**419**	**283**	**495**	**92**	**904**	***2193***

Elasmobranchs

Sharks, rays and saw fish (elasmobranchs) and bony fish were found and identified (i.e., no marine mammals or seabirds). All trenches have yielded a total of 110 isolated teeth of elasmobranchs (Fig. 2L'–O'), with four genera and families of rays (*Hypanus* whipray, *Aetobatus* eagle ray, *Pristis* saw fish, and *Rhinoptera* cownose ray) and seven species of sharks, among which five requiem sharks (*Carcharhinus* sp. and smalltail shark, *Carcharhinus porosus*; daggernose shark, *Isogomphodon oxyrhynchus*; sharpnose shark, *Rhizoprionodon* sp.; lemon shark, *Negaprion brevirostris*), a small hammer shark (scoophead, *Sphyrna media*) and a nurse shark (*Ginglymostoma cirratum*). Daggernose sharks and whiprays dominate the elasmobranch fauna in terms of specimens and occurrences (present in all sampling levels for the former [24%], in all but the trench KOU-AR6-01 for the latter [32%]; *SI Appendix*, Table S13).

Table S13. Composition of KOU-AR6 elasmobranch assemblages, earliest Late Pleistocene, Kourou, French Guiana.

	KOU-AR6-01 Grey conglo (base)	KOU-AR6-02 Grey conglo (base)	KOU-AR6-03 Grey clay (base)	KOU-AR6-03 Kaki conglo (top)	KOU-AR6-05 Kaki conglo (top)	KOU-AR6-06 Grey clays (base) >2mm	KOU-AR6-06 Grey clays (base) <2 mm	KOU-AR6-06 Kaki clays (top)	Total number per taxon	Order	Family	Common name	IUCN status
Hypanus sp.		3	8	5	2	4	12	1	35	Myliobatiformes	Dasyatidae	whipray	least concern-near threatened
Aetobatus sp.	1		1			2	2		6	Myliobatiformes	Myliobatidae	eagle rays	endangered (*A. narinari*)
Rhinoptera sp.				1			1		2	Myliobatiformes	Rhinopteridae	cownose rays	vulnerable
Pristis sp.		1							1	Rhinopristiformes	Pristidae	sawfish	critically endangered-endangered
Carcharhinus porosus	2					1	5		8	Carcharhiniformes	Carcharhinidae	smalltail shark	critically endangered
Carcharhinus sp.						1			1	Carcharhiniformes	Carcharhinidae	-	least concern-critically endangered
Isogomphodon oxyrhynchus	1	1	10	1	2	5	5	1	26	Carcharhiniformes	Carcharhinidae	daggernose shark	critically endangered
Rhizoprionodon sp.		?	2		1		2	1	6	Carcharhiniformes	Carcharhinidae	sharpnose sharks	vulnerable-near threatened
Negaprion brevirostris			2			2			4	Carcharhiniformes	Carcharhinidae	lemon shark	vulnerable
Sphyrna media	1		1			9	5		16	Carcharhiniformes	Sphyrnidae	scoophead	critically endangered
Ginglymostoma cirratum			1		1	2	1		5	Orectolobiformes	Ginglymostomatidae	nurse shark	vulnerable
Subsamples						26	33						
Number per locus	5	5	25	7	6	59		3	110				

Actinopterygians

Bony fish are mostly documented by otoliths (478 were identified; Fig. 2P'–T'), but also by bones and teeth (Fig. 2U'–W'), belonging to 35 species, 26 genera and 12 families (*SI Appendix*, Table S14). Sciaenid perciforms (16 species and 10 genera, with five species and 212 specimens of *Stellifer*) and ariid siluriforms (eight species, with *Cathorops spixii* [104 otoliths] and *Aspistor luniscutis* [44 otoliths]) widely outnumber other taxonomic groups in the sample. KOU-AR6-03 is by far the richest locality, with 425 specimens documenting 32 species, whereas taxonomic diversity is lower in KOU-AR6-01, -05 and -06, (7–10 species for only 10–38 specimens; *SI Appendix*, Table S14). The sciaenid *Macrodon ancylodon* occurs in all four localities, whereas 13 species are recognized in two or three localities, pointing to spatiotemporal homogeneity between the samples.

Table S14. Composition of KOU-AR6 bony fish assemblages, earliest Late Pleistocene, Kourou, French Guiana. Number of specimens per trench and sampled level. In red, bone and/or dental record. In black, otolith record. In bold, total number of specimens per taxon. Blue cells, marine taxa; yellow cells, freshwater taxa; green cells, marine, brackish, and freshwater taxa.

Order	Family	Species	AR6-01	AR6-03	AR6-05	AR6-06	**Total**
Albuliformes	Albulidae	*Albula vulpes*				1	**1**
Anguilliformes	Nettastomatidae	Gen. et. sp. indet.		1			**1**
Batrachoidiformes	Batrachoididae	*Thalassophryne* sp.		2	2		**4**
		Gen. et. sp. indet.			2		**2**
Characiformes	Erythrinidae	cf. *Hoplias*		4		3	**7**
Clupeiformes	Engraulidae	*Anchoa* sp.		6	3		**9**
Perciformes	Centropomidae	cf. *Centropomus*		1			**1**
	Carangidae	cf. *Selene*		1			**1**
	Sciaenidae	*Cynoscion acoupa*		2			**2**
		Isopisthus parvipinnis		1			**1**
		Larimus breviceps		3			**3**
		Lonchurus lanceolatus		5			**5**
		Macrodon ancylodon	1	25	4	3	**33**
		Macrodon atricauda		1			**1**
		Micropogonias furnieri		1			**1**
		Nebris microps		6	1	1	**8**
		Ophioscion punctatissimus		1			**1**
		Ophioscion sp.		1			**1**
		Paralonchurus brasiliensis		1			**1**
		Stellifer brasiliensis		2		1	**3**
		Stellifer menezei			4		**4**
		Stellifer gomezi		1			**1**
		Stellifer rastrifer		143	5	5	**153**
		Stellifer sp.		2			**2**
		Stellifer (lapilli)	1	44		4	**49**
Scorpaeniformes	Scorpaenidae	Gen. et. sp. Indet.		1			**1**
Siluriformes	Ariidae	*Aspistor quadriscutis*	3	2	6		**11**
		Aspistor luniscutis		40	3	1	**44**
		Bagre bagre		17			**17**
		Bagre marinus		1			**1**
		Cathorops higuchii	1		8		**9**
		Cathorops spixii	1	101		2	**104**
		Notarius grandicassis	1	2			**3**
		Gen. et. sp. indet.	2	5		2	**2/7**
	Non-Ariidae	Gen. et. sp. indet.		1			**1**
Synbranchiformes	Synbranchidae	*Synbranchus* sp.		1			**1**
		N specimens	10	425	38	23	**496**
otoliths	bones	N taxa	7	32	10	10	**35**
marine	freshwater	marine/freshwater					

3.3.3. Plantae

Charcoal

Unit A: From the bottom of the marine sequence (basal oyster-rich grey clays), 99 charcoals were hand-picked. Vitrification and/or poor preservation hampered taxonomic assignment of all charcoals from KOU-AR6-05 (khaki clays) and -06 trenches (Base, Top). Yet, cf. *Rhizophora* sp. (red mangrove, Rhizophoridae), cf. *Symphonia globulifera* (boarwood, Clusiaceae) and two representatives of Chrysobalanaceae and Myrtaceae were recognized at KOU-AR6-01, as well as branch and twig fragments of cf. *Rhizophora* sp. at KOU-AR6-03 (*SI Appendix*, Table S15).

Unit B: Tree charcoals were identified at KOU-AR6-04 Base (Fig. 3Y; *SI Appendix*, Table S15). The assemblage comprises notably *Hadroanthus* cf. *serratifolius* (ipê) and a close relative, cf. *Drypetes* sp., *Pterocarpus*-like Leguminosae, red mangrove, as well as unidentified Melastomataceae, Myrtaceae-like dicots. Today, these taxa represent trees and shrubs from the primary, riverine or dry forest, savanna or mangrove and suggest distinct vegetation succession stages at *ca.* 47 ka *cal* BP.

Unit C: Macroscopic charcoals were hand-picked at KOU-AR6-04, in several levels from Unit C, spanning the 47–1 ka time interval (MIS 3c–1). More than 60 fragments, some of them from tree stumps, were retrieved in a brown conglomerate (“Mid”), ^{14}C-dated at 47053±572 *cal* BP. They attest to the most speciose tree community uncovered here through charcoal, with at least 15 distinct tree taxa (*SI Appendix*, Table S15). *Mouriri* sp. (Melastomataceae) is the most abundant, followed by *Chaunochiton kappleri* and a close relative (Olacaceae), two close allies of *Stryphnodendron* (Leguminosae), two unidentified Chrysobalanaceae, Lecythidaceae, cf. Anacardiaceae/Burseraceae and *Handroanthus capitatus*/*serratifolius* (ipê). Just above, floodplain deposits and a silty litter dated at 43091±284 *cal* BP yielded charcoals of unidentified affinities and *Eperua* cf. *falcata* (bootlace tree, Leguminosae), respectively. The top levels, dated from the last millennia (^{14}C ages of 1938±120 and 804±55 *cal* BP), yield charcoals of unidentified Anacardiaceae/Burseraceae, hog plum (cf. *Spondias mombin*), cf. Chrysobalanaceae, *Mabea* sp. (Euphorbiaceae) in the older layer and *Eperua* cf. *falcata* (27 chunks), Rubiaceae anatomically close to *Capirona decorticans* (Batahua, 13 chunks), as well as unidentified Chrysobalanaceae and Leguminosae in the younger one.

Table S15. Composition of KOU-AR6 macrocharcoal assemblages, earliest Late Pleistocene, Kourou, French Guiana.

	Unit A					Unit B	Unit C				
Taxon	KOU-AR6-01 (10/2018, 02/2019, 04/2019)	KOU-AR6-03 (04/2019)	KOU-AR6-05, Kaki clays (04/2019)	KOU-AR6-06, Base (10/2021)	KOU-AR6-06, Top (10/2021)	KOU-AR6-04, Base	KOU-AR6-04, Mid	KOU-AR6-04, Silt litter	KOU-AR6-04, C14-1	KOU-AR6-04, Top	KOU-AR6-04, C14-2
Anacardiaceae/Burseraceae										1	
cf. Anacardiaceae/Burseraceae							1				
Chaunochiton kappleri							4				
cf. *Chaunochiton kappleri*							3				
Chrysobalanaceae	2						2				6
cf. Chrysobalanaceae	2						4			2	
cf. *Drypetes* sp.						1					
Eperua cf. *falcata*									3		27
Handroanthus capitatus/serratifolius							1				
Handroanthus cf. *serratifolius*						1					
Type *Handroanthus*						4					
type Lecythidaceae							2				
Leguminosae type 1											1
Leguminosae type 2							1				
Mabea sp.										1	
Melastomataceae						1					
Mouriri sp.							10				
cf. Myrtaceae	1					1					
Type *Pterocarpus*						1					
Rhizophora sp.						3					
cf. *Rhizophora* sp.	1	4									
cf. Rubiaceae (*Capirona decorticans*)											13
cf. *Spondias mombin*										2	
Leguminosae, type *Stryphnodendron*							1				
cf. *Symphonia globulifera*	2										
Unidentified 1	1										
Unidentified 2	1										
Unidentified 3	1										
Unidentified 4		1									
Unidentified 5										11	
Unidentified 6										2	
Unidentified 7										1	
Unidentified 8							1				
Unidentified 9							1				
Unidentified 10							1				
Unidentified 11							1				
Unidentified 12						1					
Unidentified 13						1					
Unidentifiable	27	17	4	24	11	34	29	4		42	

Total number of specimens	***38***	***22***	***4***	***24***	***11***	***48***	***62***	***4***	***3***	***62***	***47***	***325***
Minimum number of species/level	**9**	**3**	**1**	**1**	**1**	**10**	**15**	**1**	**1**	**8**	**5**	**39**
Minimum number of species/sequence			**10**			**10**			**24**			

Phytoliths

Unit A: At KOU-AR6-06, the base of the Unit A yielded phytoliths referable to unidentified woody eudicot and Asteraceae (in PN9A and PN9C pollen samples, respectively). The corresponding palynological assemblage (Fig. 3A–I), with a low pollen concentration (around 700 grains.cm^{-3}), is dominated by *Rhizophora* pollen (80 %), followed by spores of the mangrove fern *Acrostichum* (3.5 %). No *Avicennia* pollen were found. Pollen of tree species account for 9 % of the pollen sum, and reflect the influx of hinterland (Podocarpaceae, *Alnus*) and lowland (swamp) forest trees [e.g., *Iriartea*, *Catostemma* and *Symphonia* (32)]. Herb and vine pollen is relatively rare (5 %) and dominated by Poaceae and Asteraceae. Asteraceae pollen grains were only found in the PN9C sample, also containing one Asteraceae phytolith. The top of this unit has been comprehensively sampled at KOU-AR6-06 for palynomorphs and phytoliths (samples PN10–14; *SI Appendix*, Table S16). PN10–13 only provided a few phytoliths and PN10–14 was also devoid of palynological content. Grass phytoliths first occur at PN12 (dated at 104.6±17.9 ka, OSL-2), with a panicoid cross and a bilobate [C3 and C4 grasses (33, 34)], plus a fused and two rugose spheroids (woody eudicots). PN14 yielded phytolith assemblages dominated by grass phytoliths (70%), as in PN15A-B (base of Unit B, see below). PN14 had a lower concentration (<50 phytoliths) than the latter sample.

Unit B: The phytolith assemblages counted in the basal dark peat at KOU-AR6-06 (Fig. 3R –X) are dominated by grasses (65%) in both PN15A and PN15B with 65% grass, 31 and 17% woody eudicots, respectively, and almost no palm phytoliths (<1%). Most grass phytoliths encountered are from Panicoideae and Bambusoideae (*SI Appendix*, Table S16; Fig. S12). Bilobates and rondels are also common, produced by a wide array of monocot grasses (33, 34). Phytoliths from Pooideae (wavy trapezoids) and Chloridoideae (squat saddles) are rare (<1%). Strikingly, a high percentage of phytoliths were burnt (28%), especially specimens of Cyperaceae, *Heliconia* and Zingiberales. This assemblage suggests that a savanna vegetation had started growing locally way before 50 ka and spread around and settled sustainably. Previous phytolith studies showed that the natural vegetation of seasonally-flooded/coastal Holocene savannas in French Guiana consisted of Cyperaceae, Marantaceae and *Heliconia* herbs and panicoid and oryzoid grasses, with an overall high abundance of grass phytoliths (35).

Unit C: The absence of phytolith and pollen record in Unit C impedes characterizing further the last pre-Columbian seasonally-flooded local savannas (36).

***Table S16*.** Phytolith recovery from PN9–15 samples (latest Middle and Late Pleistocene), KOU-AR6-06, near the ELA4 Ariane 6 launcher pad, Kourou, French Guiana.

Site_name	Burned_phytoliths	Heliconia	Pooideae	Pharoideae	Other_palms	Conical	Spheroid	Rugose	Nodular	Ornate	Psilate	Other_Arboreal	Woody_dicots (=sum(rugose, ornate, other_arboreal))	Cyperaceae	Zingiberales (druses)	Panicoideae	Bambusoideae	Chloridoideae	Rondels	Other_grasses	Bilobates	Cross	Oryzoideae
KOU-ARG-06-PN15B	32,08	2,73	-	-	-	0,21	-	14,05	-	0,63	2,10	0,21	14,88	1,89	0,21	26,42	19,71	-	9,43	2,73	16,35	1,89	-
KOU-ARG-06-PN15A	24,45	2,44	0,24	-	-	-	-	20,54	-	2,20	6,60	1,47	24,21	1,47	0,24	14,18	8,56	0,24	7,82	3,91	28,61	0,49	-
PN15AB average	28,26	2,59	0,12	-	-	0,10	-	17,29	-	1,41	4,35	0,84	19,55	1,68	0,23	20,30	14,13	0,12	8,63	3,32	22,48	1,19	-

Site Name	Countable?	Phytoliths?	Diatoms?
KOU-ARG-06 PN15B	**yes**	17% arboreal, 65% grasses. Burnt Cyperaceae and Heliconia present. Mostly Panicoideae, few Bambusoideae	**yes**
KOU-ARG-06 PN15A	**yes**	31% arboreal, 65% grasses. Burnt Cyperaceae and Heliconia present. Mostly Panicoideae, few Bambusoideae, Pooideae, Chloridoideae	**yes**
KOU-ARG-06 PN14	no, but up to ±50 phytoliths	Similar to PN15A-B	*no*
KOU-ARG-06 PN13	*no*	1 ornate spheroid and 1 rugose spheroid (woody dicots)	*no*
KOU-ARG-06 PN12	*no*	1 fused spheroid, 2 rugose spheroids (woody dicots), 1 bilobate and 1 Panicoid cross 2	*no*
KOU-ARG-06 PN11	*no*	1 rugose spheroid (woody dicot)	*no*
KOU-ARG-06 PN10	*no*	few non-diagnostic phytoilths only (tracheids/bulliforms)	*no*
KOU-ARG-06 PN9D	*no*	-	*no*
KOU-ARG-06 PN9C	*no*	Asteraceae	*no*
KOU-ARG-06 PN9B	*no*	-	*no*
KOU-ARG-06 PN9A	*no*	1 rugose spheroid (woody dicot)	*no*

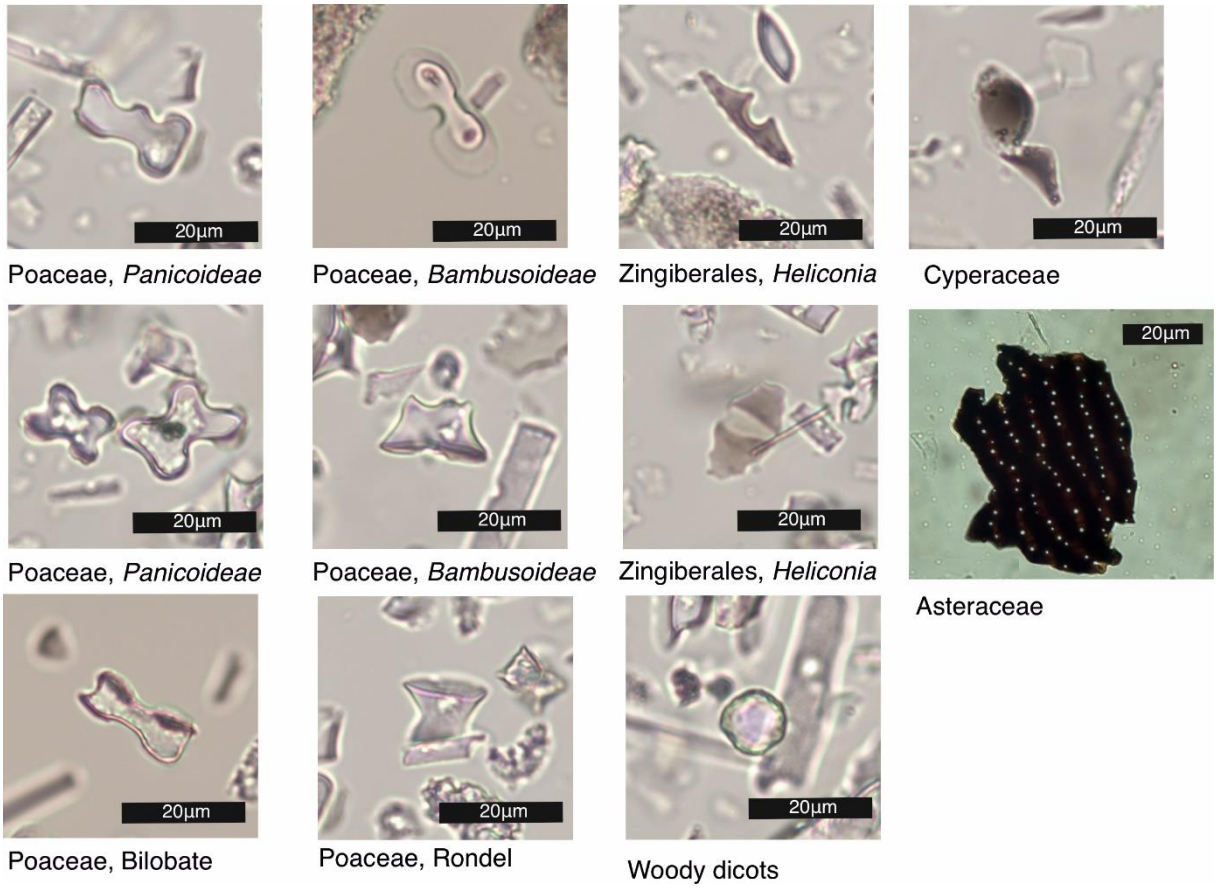

Fig. S12. Selected phytoliths from PN15 (Late Pleistocene), KOU-AR6-06, near the ELA4 Ariane 6 launcher pad, Kourou, French Guiana.

Pollen

Unit A: The sample PN6, located at 1.4 m ASL, yielded high amounts of *Rhizophora* mangrove pollen, including clumps, which suggest the proximity of a mangrove belt.

Unit B: The pollen concentration of the PN15 sample is much higher than in Unit A (around 20,600 grains.cm^{-3}), with a high relative abundance of Poaceae (49 %) and Spermacoceae (36 %) pollen, indicators of open and disturbed vegetation (Fig. 3L–Q) prior to 45 ka *cal* BP in the ELA4 area (Fig. 4B). Many Poaceae pollen grains are relatively large (50–64 µm), furthering the presence of Panicoideae and Bambusoideae grass phytoliths. Mangrove (2.4 %) and tree (3.5 %) pollen are rare (*SI Appendix*, Table S17). Conversely, the large amount of charred plant fragments (“microcharcoals”) in the pollen slides is notable. The high number of macro-charcoals and high percentage of burned phytoliths indicate recurring fires at the site during the concerned time interval, i.e., prior to 47 ka *cal* BP (age of the base of the overlying Unit C; see below), and further consistent with a glacial stadial (MIS 4: 72–58 ka; Fig. 4).

Unit C: The absence of phytolith and pollen record in Unit C impedes characterizing further the last pre-Columbian seasonally-flooded local savannas (36).

Table S17. Composition of KOU-AR6-06 pollen assemblages, early Late Pleistocene, Kourou, French Guiana.

KOU-AR6				KOU-AR6-PN9	(%)	KOU-AR6-PN15	(%)
		Lycopodium/cm3		18407		18407	
		Lycopodium		8650		334	
		pollen sum		323		374	
		pollen conc. (grains/cm3)		687		20611	
group							
1	Acanthaceae	*Avicennia*	mangrove, tree	0	0,0	0	0,0
1	Pteridaceae	*Acrostichum*	mangrove, fern	11	3,4	0	0,0
1	Rhizophoraceae	*Rhizophora*	mangrove, tree	257	79,6	9	2,4
2	Arecaceae	*Attalea* type	palm tree	3	0,9	1	0,3
2	Arecaceae	*Iriatea*	palm tree	1	0,3	0	0,0
2	Arecaceae	*Prestoea* type	palm tree	1	0,3	0	0,0
3	Anacardiaceae	undiff.	tree	1	0,3	0	0,0
3	Aquifoliaceae	*Ilex*	tree	1	0,3	0	0,0
3	Araliaceae	*Schefflera*	tree	1	0,3	1	0,3
3	Betulaceae	*Alnus*	tree	1	0,3	0	0,0
3	Burseraceae	*Protium*	tree	3	0,9	0	0,0
3	Chloranthaceae	*Hedyosmum*	tree	3	0,9	0	0,0
3	Clusiaceae	*Symphonia*	tree	1	0,3	0	0,0
3	Euphorbiaceae	*Mabea*	tree	0	0,0	1	0,3
3 cf.	Malpighiaceae	*Byrsonima*	tree	0	0,0	7	1,9
3	Malvaceae	*Catostemma*	tree	1	0,3	0	0,0
3	Malvaceae	*Pachira*	tree	0	0,0	0	0,0
3	Melastomataceae	*Mouriri*	tree	1	0,3	0	0,0
3 cf.	Meliaceae	*Trichilia*	tree	2	0,6	0	0,0
3	Myristicaceae	*Virola*	tree	0	0,0	0	0,0
3	Myrtaceae	undiff.	tree	6	1,9	1	0,3
3	Podocarpaceae	*Podocarpus*	tree	1	0,3	0	0,0
3	Polygonaceae	*Symmeria*	tree	0	0,0	0	0,0
3	Urticaceae	*Cecropia*	tree	0	0,0	0	0,0
3	Urticales	undiff.	tree	1	0,3	0	0,0
4	Asteraceae	undiff.	herb	4	1,2	29	7,8
4	Asteraceae	*Vernonia* type	herb	0	0,0	0	0,0
4	Convolvulaceae	*Ipomoea*	herb/vine	0	0,0	0	0,0
4	Euphorbiaceae	*Acalypha*	herb	1	0,3	0	0,0
4	Gentianaceae	*Schultesia*	herb	0	0,0	1	0,3
4	Malvaceae	*Peltaea*	herb/vine	3	0,9	0	0,0
4	Poaceae	undiff.	herb	6	1,9	186	49,7
4	Rubiaceae	Spermacoceae	herb	0	0,0	137	36,6
4	Verbenaceae	*Petrea*	herb/vine	1	0,3	0	0,0
5	Apiaceae	undiff.	undefined	1	0,3	1	0,3
5	Bignoniaceae	undiff.	undefined	1	0,3	0	0,0
5	Fabaceae (P)	undiff.	undefined	1	0,3	0	0,0
5	Malpighiaceae	undiff.	undefined	3	0,9	0	0,0
5	Melastomataceae/ Combretaceae	undiff.	undefined	1	0,3	0	0,0
5	Proteaceae	undiff.	undefined	0	0,0	0	0,0
5 cf.	Rubiaceae	*Alseis*	undefined	2	0,6	0	0,0
5	Rutaceae	undiff.	undefined	1	0,3	0	0,0
5	Salicaceae	undiff.	undefined	2	0,6	0	0,0
			mangrove		83,0		2,4
			trees		8,7		2,9
			herbs/vines		4,6		94,4
			undefined		3,7		0,3
			total		100,0		100,0

4. Recent referential for marine taxonomic diversity of metazoans

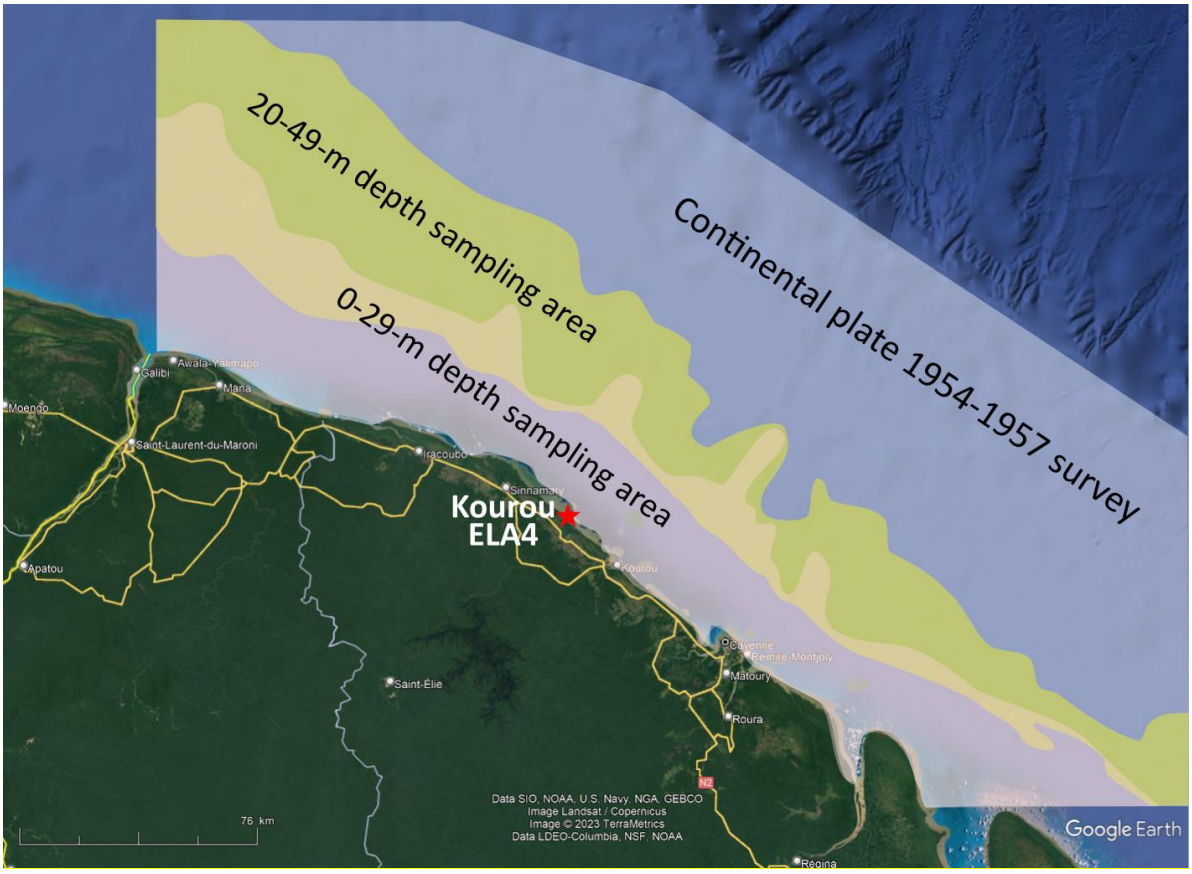

Fig. S13. Map of the sampling survey for recent marine invertebrates and bony fish, performed in 1954–1957 on the Guianese continental plate. Four hundred samples were caught on a *ca.* 40,000-km2 area and at a 0–105-m depth, among which 66 and 234 samples at 0–24 and 25–49-m depth ranges, respectively. Sampling areas coincide with those depicted by (37). Background from Google Earth®.

Table S18. Comparison of taxonomic diversity per metazoan group, between the 1954–1957 survey on recent organisms [(37); see ***Fig S13*** above] and the Kourou ELA4 sampling effort, in the early Late Pleistocene of Kourou, French Guiana (this work), detailing species/generic diversity depending on the depth range (between brackets) and type of substrate, when available. Mud: 0–30-m depth, 110 samples; muddy sands: 20–49-m depth, 272 samples; dead shells: 20–49-m depth, 272 samples; sands: 20–49-m depth, 272 samples); Last Interglacial (LIG) diversity is measured through five samples from a 0.5 km^2 area. White/yellow/green cells denote lower/similar/higher diversity between LIG and recent samples.

		Recent diversity (Guianese continental plate): species/genera				LIG diversity
Taxonomic groups		mud (0-30 m)	muddy sands (20-49 m)	dead shells (20-49 m)	sands (20-49 m)	muddy sands (5-10 m)
Corals		0/0	1/1			1/1
Mollusks	Gastropods	13/11				50/44
	Bivalves	20/16				35/35
	Scaphopods	1/1				2/2
Decapods	Brachyurans	10/7	-	5/5	8/8	5/5
Echinoderms	Sea stars	2/2	4/3	4/3	4/3	1/1
	Urchins	0/0	0/0	4/4	3/3	3/3
Bony fish		35/31	40/37	41/35	30/26	35/26
	Total	**81/68**	**79/69**	**89/76**	**80/69**	**132/117**

5. PAUP Buffer

```
P A U P *
Version 4.0a (build 169) for 32-bit Microsoft Windows (built on Feb 10 2021 at 22:12:44)
Thu Dec 28 16:29:05 2023

        ------------------------------NOTICE-----------------------------
          This is a test version that is still changing rapidly.
          Please report bugs to dave@phylosolutions.com
        -----------------------------------------------------------------

Running on Intel(R) Core(TM) i5-7200U CPU @ 2.50GHz
    Current processor contains 2 CPU cores on 1 socket (hyperthreaded to 4 logical cores)
    Executable built for IA-32 architecture (64-bit word length)
    SSE vectorization enabled
    SSSE3 instructions supported
    Multithreading enabled using Pthreads

Processing of file "C:\Users\pierr\Documents\Publications\En cours\Kourou ELA4
assemblage\R2\Antoine-et-al_SI-Appendix4_R2.nex" begins...

Data matrix has 7 taxa, 74 characters
Valid character-state symbols: 01
Missing data identified by '?'
Gaps identified by '-'

*** Skipping "NOTES" block

Processing of input file "Antoine-et-al_SI-Appendix4_R2.nex" completed.

paup> set criterion=distance;

Optimality criterion set to distance.

paup> UPGMA;

UPGMA search settings:
  Ties (if encountered) will be broken systematically
  Distance measure = mean character difference
  74 characters are included
  All characters have equal weight
  (Tree is rooted)

UPGMA tree:
```

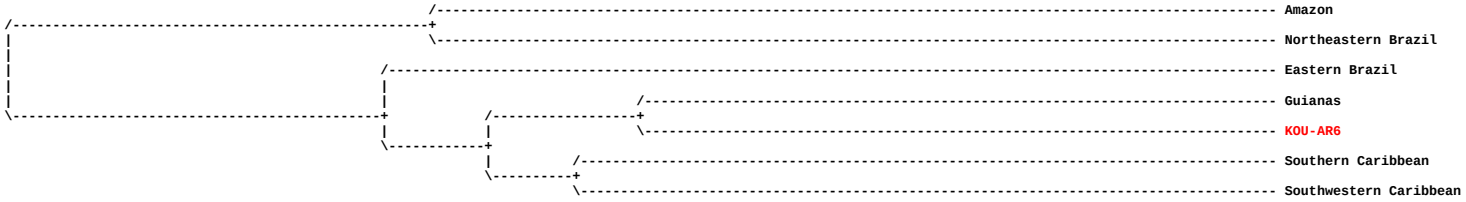


```
Tree found by UPGMA method stored in tree buffer
Time used for tree calculation = 0.00 sec (CPU time = 0.00 sec)


paup> set criterion=parsimony;

Optimality criterion set to parsimony.

paup> set rootMethod=midpoint;

paup> allTrees;
```

Exhaustive search settings:
  Optimality criterion = parsimony
    Character-status summary:
      Of 74 total characters:
        All characters are of type 'unord'
        All characters have equal weight
        3 characters are constant (proportion = 0.0405405)
        14 variable characters are parsimony-uninformative
        Number of parsimony-informative characters = 57
    Gaps are treated as "missing"
  Initial 'Maxtrees' setting = 100
  Branches collapsed (creating polytomies) if maximum branch length is zero
  'MulTrees' option in effect
  No topological constraints in effect
  Trees are unrooted

Exhaustive search completed:
  Number of trees evaluated = 945
  Score of best tree found = 117
  Score of worst tree found = 153
  Number of trees retained = 1
  Time used = 0.00 sec (CPU time = 0.00 sec)

paup> describeTrees;

Tree description:

  Unrooted tree(s) rooted using midpoint method
  Optimality criterion = parsimony
    Character-status summary:
      Of 74 total characters:
        All characters are of type 'unord'
        All characters have equal weight
        3 characters are constant (proportion = 0.0405405)
        14 variable characters are parsimony-uninformative
        Number of parsimony-informative characters = 57
    Gaps are treated as "missing"
    Character-state optimization: Minimum F-value (MINF)

Tree 1 (rooted using midpoint method)

Tree length = 117
Consistency index (CI) = 0.6068
Homoplasy index (HI) = 0.3932
CI excluding uninformative characters = 0.5534
HI excluding uninformative characters = 0.4466
Retention index (RI) = 0.4713
Rescaled consistency index (RC) = 0.2860

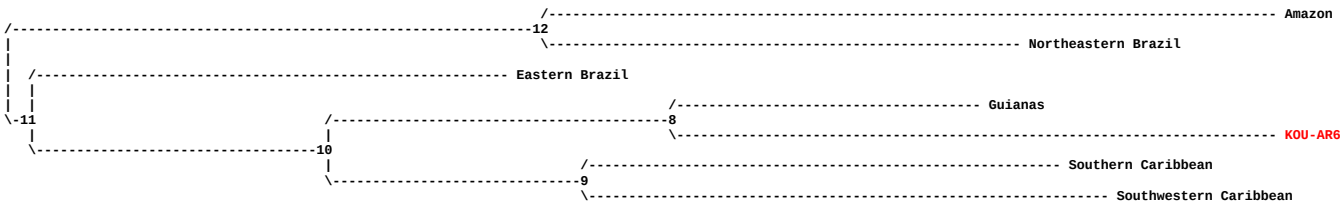

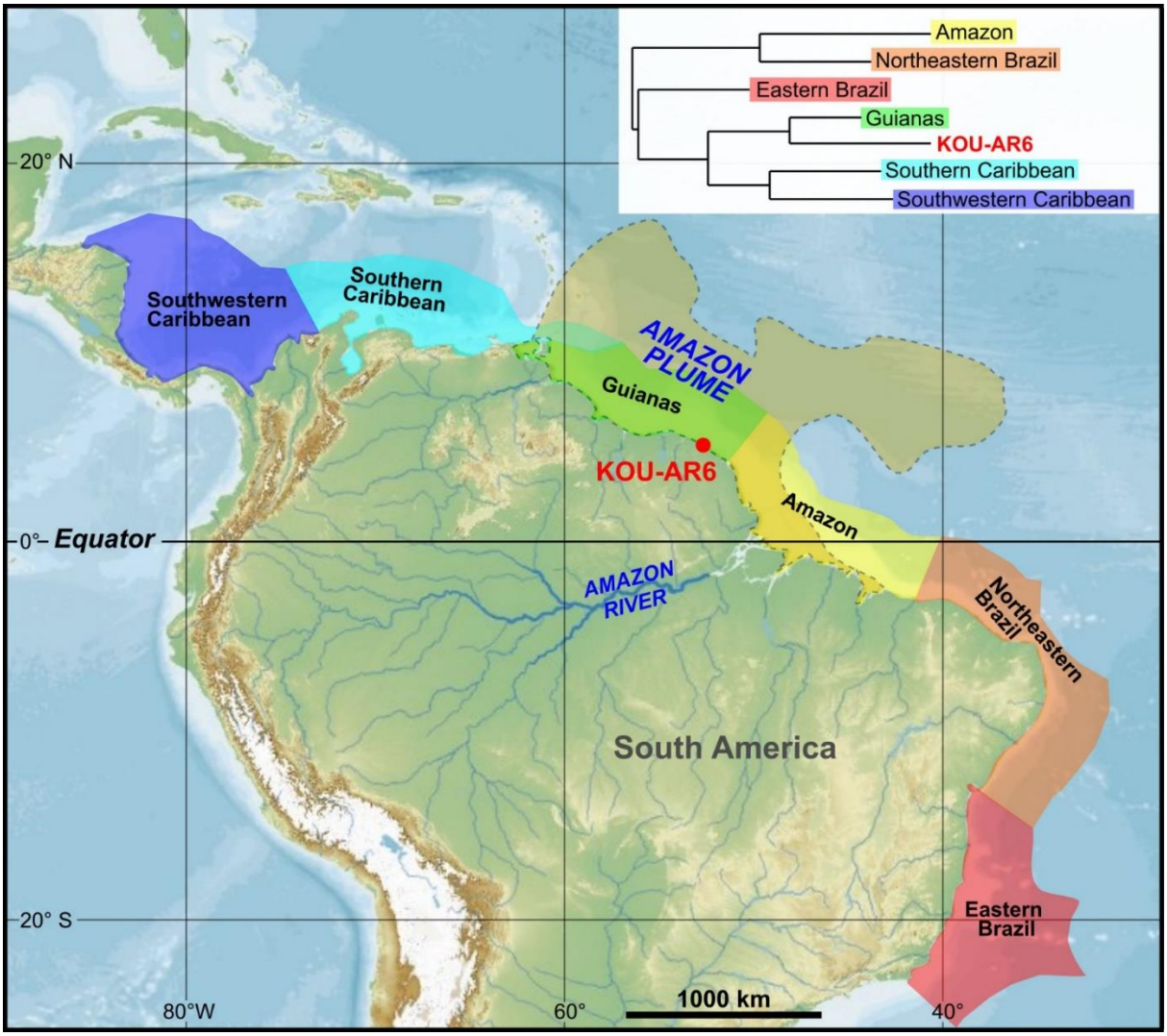

Fig. S14. Biogeographic map of the tropical Western Atlantic with coastal areas considered in Giachini Tosetto et al. (38) and taxon-related data extracted from both Ocean Biodiversity Information System repository (https://mapper.obis.org), the Malacolog Version 4.1.1 Database (http://www.malacolog.org/wasp.php?mode=locality) of Western Atlantic Marine Mollusca, and a monograph on French Guiana's mollusks (39). Superimposed white box stands for cluster dendrogram analysis depicting the overall similarity between the Last Interglacial KOU-AR6 fossil mollusk assemblage and the recent mollusk communities from six contiguous coastal areas of the tropical Western Atlantic. The corresponding topology was obtained through distance analysis (UPGMA) and parsimony analysis (using mid-point rooting method). Ecological conditions were more similar between KOU-AR6 and the Guianas, and the Southern + Southwestern Caribbean, than with Eastern Brazil and, to a wider extent, with Northeastern Brazil and Amazon coastal waters today. This pattern suggests that the Amazon Plume was not acting as a strong ecological barrier in coastal areas of the Guianese continental shelf by Last Interglacial times, in stark contrast to today's pattern.

SI References

1. R. Scheel-Ybert, Charcoal collections of the world. *IAWA Journal* **37**, 489–505 (2016).
2. InsideWood, Published on the Internet. (2004-onwards). [http://insidewood.lib.ncsu.edu/search; accessed in July 2020].
3. E. A. Wheeler, Inside Wood–A web resource for hardwood anatomy. *Iawa Journal* **32**, 199–211 (2011).
4. S. C. Bodin, *et al.*, CharKey: An electronic identification key for wood charcoals of French Guiana. *IAWA Journal* **40**, 75–S20 (2019).
5. C. N. H. McMichael *et al.*, 30,000 years of landscape and vegetation dynamics in a mid-elevation Andean valley. *Quatern. Sci. Rev.* **258**, 106866 (2021).

6. C. Crifò, C.A. Strömberg, Small-scale spatial resolution of the soil phytolith record in a rainforest and a dry forest in Costa Rica: applications to the deep-time fossil phytolith record. *Palaeogeogr., Palaeoclimatol., Palaeoecol*. **537**, 109107 (2020).
7. K. Neumann *et al.*, International Code for Phytolith Nomenclature (ICPN) 2.0. *Ann. Botany* **124**, 189–199 (2019).
8. D. R. Piperno, *Phytoliths: a comprehensive guide for archaeologists and paleoecologists*. Rowman Altamira (2006).
9. K. Feagri, J. Iversen, *Textbook of Pollen Analysis* (fourth ed.), Wiley, London (1989).
10. S.E. Lowick *et al.*, Luminescence dating of Middle Pleistocene proglacial deposits from northern Switzerland: methodological aspects and stratigraphical conclusions. *Boreas* **44**, 459–482 (2015).
11. A.S. Murray, A.G. Wintle, Dating quartz using an improved single-aliquot regenerative-dose (SAR) protocol. *Radiation Measur*. **32**, 57–73 (2000).
12. Murray, A.S., A.G. Wintle, The single aliquot regenerative dose protocol: potential for improvements in reliability. *Radiation Measur*. **37**, 377–381 (2003).
13. Duller, G.A.T., Distinguishing quartz and feldspar in single grain luminescence measurements. *Radiation Measur*. **37**, 161–165 (2003).
14. F. Preusser, H.U. Kasper, Comparison of dose rate determination using high-resolution gamma spectrometry and inductively coupled plasma-mass spectrometry. *Ancient TL* **19**, 17–21 (2001).
15. J.A. Durcan, G.E. King, G.A.T. Duller, DRAC: Dose Rate and Age Calculator for trapped charge dating. *Quatern. Geochronol.* **28**, 54–61 (2015).
16. S. Kreutzer, C. Schmidt, M. Fuchs, M. Dietze, Introducing an R package for luminescence dating analysis. *Ancient TL* **30**, 1–8 (2012).
17. R.F. Galbraith *et al.*, Optical dating of single and multiple grains of quartz from Jinmium rock shelter, northern Australia: part i, experimental design and statistical models. *Archaeometry* **2**, 339–364 (1999).
18. J. Fietzke *et al.*, Determination of uranium isotope ratios by multi-static MIC-ICP-MS: Method and implementation for precise U- and Th-series isotope measurements. *J. Anal. At. Spectrom*. **20**, 395–401 (2005)
19. C.D. Woodroffe *et al*., Stratigraphy and chronology of late Pleistocene reefs in the Southern Cook Islands, South Pacific. Quat. Res. 35, 246-263 (1991).
20. P. Vermeesch, IsoplotR: a free and open toolbox for geochronology. *Geosci. Frontiers* **9**, 1479–1493 (2018).
21. C. Paton *et al.*, Iolite: Freeware for the visualisation and processing of mass spectrometric data. *J. Analyt. Atomic Spectrom*. **26**, 2508–2518 (2011).
22. C. Carcaillet, B. Talon, Aspects taphonomiques de la stratigraphie et de la datation de charbons de bois dans les sols : exemple de quelques sols des Alpes. *Géogr. Phys. Quatern.* **50**, 233–244 (1996).
23. M.B. Schiffer, Radiocarbon dating and the “old wood” problem: the case of the Hohokam chronology. *J. Archaeol. Sci.* **13**, 13–30 (1986).
24. M. Molnar *et al.*, Status Report of the New AMS 14C Sample Preparation Lab of the Hertelendi Laboratory of Environmental Studies (Debrecen, Hungary). *Radiocarbon* **55**, 665–676 (2013).
25. C. Bronk Ramsey, OxCal v. 4.4.4. (2021) [https://c14.arch.ox.ac.uk/oxcal.html]
26. P. Reimer *et al*., The IntCal20 Northern Hemisphere radiocarbon age calibration curve (0–55 cal kBP). *Radiocarbon* **62**, 725–757 (2020).
27. A.G. Wintle, Luminescence dating: where it has been and where it is going. *Boreas* **37**, 471–482 (2008).
28. N. Sariaslan, M.R. Langer, Atypical, high-diversity assemblages of foraminifera in a mangrove estuary in northern Brazil. *Biogeosci*. **18**, 1–18 (2021).
29. A.C.S. Almeida, F.B.C. Souza, L.M. Vieira, Malacostegine bryozoans (Bryozoa: Cheilostomata) from Bahia State, northeast Brazil: taxonomy and non-indigenous species. *Marine Biodiv.* **48**, 1463–1488 (2017).
30. L.M. Vieira, A.E. Migotto, J.E. Winston, Synopsis and annotated checklist of Recent marine Bryozoa from Brazil. *Zootaxa* **1810**, 1–39 (2008).
31. D.J. Hughes, J.B.C. Jackson, Do constant environments promote complexity of form?: The distribution of bryozoan polymorphism as a test of hypotheses. *Evolution* **44**, 889–905 (1990).
32. T. Van der Hammen, A palynological study on the Quaternary of British Guiana. *Leidse Geol. Meded*. **29**: 125–180 (1963).
33. D. R. Piperno, *Phytoliths: a comprehensive guide for archaeologists and paleoecologists*, (Rowman Altamira, 2006).
34. C. Crifò, C. A. Strömberg, Small-scale spatial resolution of the soil phytolith record in a rainforest and a dry forest in Costa Rica: applications to the deep-time fossil phytolith record. *Palaeogeogr., Palaeoclimatol., Palaeoecol.* **537**, 109107 (2020).

35. J. Iriarte *et al.*, Late Holocene Neotropical agricultural landscapes: phytolith and stable carbon isotope analysis of raised fields from French Guianan coastal savannahs. *J. Archaeol. Sci.* **37**, 2984–2994 (2010).
36. J. Iriarte *et al.*, Fire-free land use in pre-1492 Amazonian savannas. *Proc. Natl. Acad. Sci. U.S.A.* **109**, 6473–6478 (2012).
37. Durand, J. Les éléments principaux de la faune et leurs relations avec le fond, *Cahiers de l'ORSTOM* **3**, 1–93 (1959).
38. Giachini Tosetto, E. *et al.*, The Amazon River plume, a barrier to animal dispersal in the Western Tropical Atlantic. *Scientific Reports* **12**, 537 (2022).
39. Massemin, D., D. Lamy, J.-P. Pointier, O. Gargominy, Coquillages et escargots de Guyane. *Publications Scientifiques du Muséum*, MNHN, Paris (2009).